EFFECT OF SURFACE ROUGHNESS ON TYRE CHARACTERISTICS

Carl Becker[a] and Schalk Els[a]

[a] *University of Pretoria, 1 Lynnwood Road, Pretoria, 0002, SOUTH AFRICA*

carl.becker@up.ac.za, schalk.els@up.ac.za

Tyre characterisation is not a trivial or inexpensive exercise thus it is important to obtain representative measurements during tyre characterisation tests. Different test methods exist and vary from laboratory tests to outdoor tests on different surfaces. Each of the test surfaces have different surface roughness and will result in different tyre characteristics. This study compares friction coefficient measurements on dry non-deformable surfaces for laboratory test surfaces and outdoor test tracks on the same agricultural tyre with large lugs at two inflation pressures and three tread wear conditions. The influence of surface roughness on friction coefficient is investigated. The macrotexture and microtexture of multiple surfaces are measured and compared. The importance of measuring the microtexture of the outdoor test surface is noted. Static/Non-rolling tyre tests in a laboratory are compared to Static/Non-rolling tyre tests as well as Dynamic/Rolling tyres tests at an outdoor test facility. Excellent correlation is found between the Static vs. Dynamic and laboratory vs. outdoor tests results when the laboratory tests are conducted on a surface representing the outdoor surface.

Keywords: agricultural tyre, tyre wear, friction coefficient, tyre test, surface roughness, microtexture, macrotexture

1. Introduction

Simulation results are only as reliable as the input data and in vehicle ride or handling simulations the primary excitation into the vehicle is via the tyres, thus the importance of having reliable tyre data for accurate tyre modelling and vehicle simulation. With the tyres being the only

suspension on many agricultural and construction vehicles, the importance of accurate tyre models is even more critical. The advances made in tyre technology to date have placed a large question mark on the reliability on the limited historical collection of tyre data available especially in the agricultural and construction industry. Other vehicle factors that are affected by the tyre characteristics range from off-road traction and soil compaction to on-road handling, ride comfort, braking and motion resistance.

The FTire model is a physics-based flexible structure tyre model developed by cosin scientific software (2017). The model can be used for handling and ride comfort simulations on rough terrain. The FTire model can be parameterized at two inflation pressures with the use of static tests to obtain vertical stiffness (on flat surface and cleats), lateral stiffness and longitudinal stiffness together with footprints and tyre geometry. Modal analysis will contribute to model parameterisation but it is not an essential requirement. Damping over cleats and dynamic tests in the form of lateral force vs. slip angle and longitudinal force vs. % longitudinal slip are used for validation. The required tests can be conducted on a flat track or drum tester. The FTire is a very flexible/adjustable tyre model and enables the user to adjust the amount of tread on the belt and inflation pressure amongst other parameters.

Tyre characteristics can be measured using multiple methods. Each method has different constraints and have their own set of positives and negatives features. This is the case for passenger cars, sports cars, motorcycles, commercial trucks, heavy duty trucks, agricultural and construction vehicles. Many test laboratories are spread worldwide and all have the capability to parameterize relatively small tyres. Testing larger tyres have its own challenges as one needs large amounts of driving power and infrastructure to test these tyres at the designed loads. Typical indoor laboratory test rigs include drum test rigs or flat track rigs. Some test rigs can only be used for traction

characterisation, where other test rigs can conduct lateral force vs. slip angle tests, motion resistance measurements or even simulate track racing conditions. These laboratory test rigs tend to have different test surfaces (corundum surfaces/sandpaper or steel belts) and on some of these test rigs the test surface can be changed.

The Vehicle Dynamics Group (VDG) in the Department of Mechanical and Aeronautical Engineering of the University of Pretoria in South Africa, has developed a Dynamic Tyre Test Trailer (DTTT) and a Static Tyre Test Rig (STTR) as described by Becker and Els (2018). The DTTT tests rolling tyres with diameters larger than 800mm and up to 2000mm, where two of the same tyres are tested in opposed lateral slip directions up to a maximum vertical load of 50kN per wheel. The DTTT can measure tyre forces and moments for lateral force vs. slip angle measurements, longitudinal force vs. longitudinal slip measurements as well as combined lateral and longitudinal force measurements during braking at pre-determined lateral slip angles. The STTR can measure the static stiffness of a tyre in the longitudinal or lateral direction for a predetermined vertical load on test surfaces that are interchangeable. The STTR is equipped with 1MN actuators and can accommodate 4000mm diameter tyres.

The University of Hohenheim, has multiple large tyre test rigs in the form of a flat belt test stand, single wheel test trailer and an instrumented test tractor as presented by Witzel (2018). These test rigs/platforms can be used to measure longitudinal forces, lateral forces and motion resistance on larger agricultural tyres. Other single wheel test trailers have been built for agricultural tyres, used and upgraded from early 1960's to present. These trailers can be used on any terrain. Billington (1973) introduced the NIAE MkII single wheel tester in 1973. Ambruster and Kutzbach

(1989), developed a single wheel tester which parameterized a driven wheel at pre-set slip angles. Shmuleviuch et al. (1996) presented a new field single wheel tester. These trailers can be used on any terrain. This adds an additional variable in the form of the surface roughness of the terrain, which effects the friction coefficient and is not constant in field/ outdoor tests and varies between locations. This led to the current investigation where multiple test surfaces are characterised, the friction characteristics of a tyre is measured on test surfaces and results compared. This is followed by laboratory and outdoor tests with the same tyre on a surface with similar roughness characteristics. The findings for this analysis are discussed in this paper.

2. Surface Roughness Effects on Friction Coefficient

Multiple studies have been conducted in measuring the friction coefficient of tyres and measuring the surface roughness of a specific terrain, however no research could be found where the same tyre was characterized in a laboratory on different surfaces and compared to outdoor tests on similar surfaces with all of the surface roughness compared. Persson (2001), has indicated that different testing velocities results in different friction coefficients, higher velocities result in a lower friction coefficient, and flash temperature has a significant effect on the friction coefficient. These variables can be controlled to a degree between laboratory tests and outdoor tests. Methods such as the grease sample, sand patch, outflow meters, British Pendulum and circular track meters are methods used to measure the texture and friction coefficient of a terrain. Salehi et.al (2019), did a comprehensive study to determine the rubber friction on multiple grain sizes corundum surfaces on a Laboratory Abrasion Tester and found that a corundum disc with disc designation 180 correlated to friction coefficient measurement on a test track in Europe. The surface roughness of the European test track was unfortunately not stated.

The basic friction mechanism of dry relative motion between the tyre and the road is generated by a combination of adhesion and hysteresis effects, as described by Gillespie (1992) and Salehi et.al, (2019). The total longitudinal friction force can be written as:

$$F = F_{adhesion} + F_{hysteresis} \qquad \text{eq. (1)}$$

The adhesion occurs in the real contact area, particularly the fine-scale texture below 0.5mm on self-affine fractal surfaces (microtexture), it is generally noted that the softer the rubber compound and higher the vertical force, F_z on the tyre, the larger the effect of adhesion as a larger contact area is achieved due to the rubber deforming around the terrain. The smoother the terrain the larger the adhesion component is in the total friction force. The hysteretic component results from the internal friction of the rubber. During sliding, the asperities of the rough terrain exert oscillating forces on the rubber surface, leading to cyclic deformations of the rubber, and energy dissipation via the internal damping of the rubber. Because of its low elastic modulus, rubber often exhibits elastic instabilities during sliding. This involves the compressed rubber surface in front of the contact area undergoing a buckling which produces detachment waves which propagate from the front-end to the back-end of the contact area. These are the so called Schallamach waves, (Persson 2001), and is the cause of the stick-slip phenomena predominantly seen on smoother surfaces. This phenomenon is observed during testing in the study and has a greater effect on the large off-road tyres as the tread blocks, on the tyres of interest, are very large with a small percentage of rubber in contact with the surface when the tyre is new.

The surface texture characteristics of a pavement has a direct relation to the friction properties. These surface texture characteristics are known as megatexture, macrotexture and microtexture,

which describes different wavelengths in the terrain profile, as described in the International Organization for Standardization, ISO 13473-1:1997. The megatexture describes wavelengths from 0.5m to 50mm (2 to 20 cycles/m). The macrotexture is associated with the roughness of the road surface that effects the water drainage from the tyre footprint, where the surface deviations have wavelengths from 50mm to 0.5mm (20 to 2000 cycles/m). The microtexture varies from harsh to polished and effects the friction coefficient at low speeds where it depends mainly on the adhesion effects. These surface deviations have wavelengths less than 0.5mm and are measured at a micron scale (Ergun et.al, 2005). Measuring the macro- and microtextures require two different measuring devices. During this study a XY table fitted with an AR700 Acuity road profiling laser (Acuity, 2015), was used to measure the macrotexture of the surfaces, as shown in Figure 1, by scanning 10 longitudinal lines equally spaced in the lateral direction as indicated by the red lines in Figure 1b). The smallest wavelength is limited by the diameter of the dot size of the laser which is 120µm. The longest wavelength was defined by the travel of the XY table which was 200mm. The XY table used to measure the macrotexture is fully mobile and was used to measure the macrotextures of all the laboratory and outdoor test surfaces used in this study. The special frequency range covered by the XY table was from 5 to 8333 cycles/m, which covers a wide spectrum from a section of megatexture to microtexture.

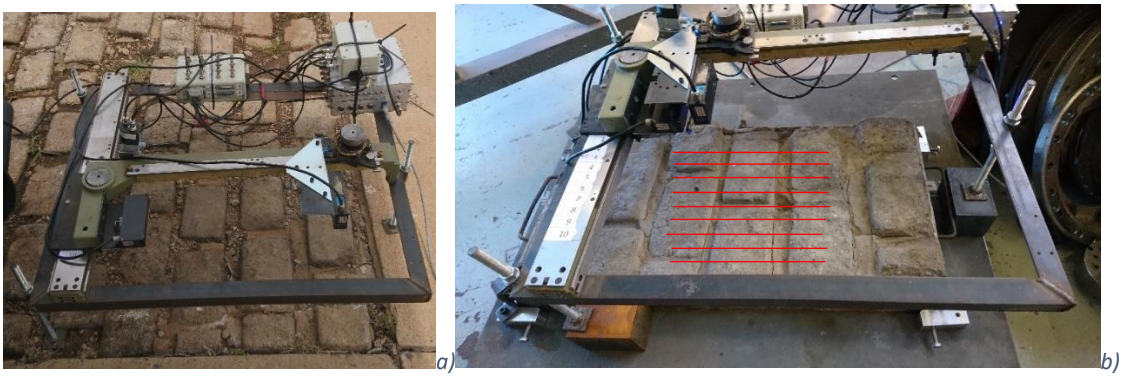

Figure 1:Macroprofiler measuring on a) Outdoor Belgian paving section b)Laboratory casting of Belgian Paving.

The microtextures were measured with an engineering stylus in the form of a Mitutoyo SJ-210 portable surface roughness tester (Mitutoyo, 2021), as shown in Figure 2, that is able to measure the surface roughness according to the ISO 4287:1997. The sample length of these microtexture profiles are 4mm with and average pitch of 0.5µm. This covers the special frequency range of 2500 to 2 000 000 cycles/m, which gave a good overlap with the measurements taken using the XY table.

Figure 2: Micro profiler a)On Asphalt surface macrotexture scale b)Close-up for microtexture scale .

The roughness of a test course can be specified with the use of the Root Mean Square elevation (RMS) in the time domain or a Displacement Spectral Density (DSD) in the frequency domain (Gorsich et.al., 2003), and the roughness of a terrain is characterized according to ISO 8608:1995.

The RMS of the vertical displacement of the profile and the square root of the area under the displacement spectral density should result in the same value. The Power Spectral Density (PSD) of a signal describes how the power of a signal or a time series is distributed in the frequency domain. The same can be done for the displacement; consequently, the Displacement Spectral Density of a signal describes how the displacement of a signal or a time series is distributed in the frequency domain.

The ISO 8608:1995 specifies a uniform method of reporting measured vertical road profile data for either one-track or multiple-track measurements. It applies to the reporting of measured vertical profile data taken on roads, streets and highways and on off-road terrain. The standard provides general guidance for the use of road profile statistical data for simulation studies and for related studies such as evaluation of comfort, suspensions and road profiles. The ISO standard defines different road classifications. These classifications are supplied in the form of class limits for the DSD for different classes of roads. The classes range from a class-A road which is a smooth road to a class-H road which is a very rough road. The DSD of a random road, plotted on a log-log scale, forms a straight line and may be described by the power function.

$$S_z = A\varphi^{-n} \qquad \text{eq. (2)}$$

Where S_z is the vertical DSD, n is the road index, A is the roughness coefficient at a spatial frequency of 1cycle/m and φ is the spatial frequency measured in cycles/m. The road index parameter is calculated with a spatial frequency window from 0.05 to 10 cycles/m (megatexture). The ISO 8606:1995 specifies that for off-road profiles the reported spatial frequency range for φ should be from 0.05 cycles/m (wavelength = 20m) to 10 cycles/m (wavelength = 0.1m) as the tyre

creates an enveloping effect that filters the road vibration input. This straight line on a log-log scale extends to the macrotexture, however the gradient for the microtexture increases.

Another method for calculating the DSD was described by Zaayman (1988). In this method the DSD $S_{xx}(\delta)$ of the road was calculated by dividing the squared Fast Fourier Transform (FFT) X_δ of the road profile $x(d)$ by twice the step-in frequency ΔF,as shown in eq.(3):

$$S_{xx}(F) = \frac{|X_\delta(F)|^2}{2\Delta F} \qquad \text{eq. (3)}$$

The squared FFT is equivalent to the FFT of the road profile X_δ multiplied with the complex conjugate of X_δ.

$$|X_\delta(F)|^2 = X_\delta X_\delta{}^* \qquad \text{eq. (4)}$$

This method is used by Becker and Els, (2014), for calculating the DSD of the measured profiles of the test tracks at the Gerotek Test Facilities, (Gerotek Test Facilities, 2021), the same method is used for calculating the DSD of the measured profiles in this study.

Scholtz and Els (2020) showed that the Heinrich/ Klüppel friction model, (Heinrich and Klüppel, 2008), can be used to estimate the friction coefficient for both smooth and rough concrete surfaces. This model was compared to measured friction coefficient using the Da Vinci method (American Institute of Physics, 2015), where the friction coefficient is determined mathematically by dividing the longitudinal force by the normal force as shown below in eq. (5):

$$\mu = \frac{\text{Longitudinal Force}}{\text{Normal Force}} = \frac{F_x}{F_z} = \frac{ma}{mg} \qquad \text{eq. (5)}$$

The same Belgian paving concrete test section as tested by Scholtz and Els (2020) is also used in this study. In this study friction coefficient is calculated from measured vertical/normal force and longitudinal force as described in eq. (5).

3. Roughness Measurements on Test Surface

The surface roughness of all the test surfaces tested in this study was profiled with the macrotexture profiler and with the microtexture profiler as described in section 2. To ensure that microtexture of the same surface is profiled over which the friction coefficient measurements were conducted, a template was made with 21 measuring points that replicated the contact patch of the tyre as shown in Figure 3. This template was placed in the same location as the contact patch on all STTR test surface as shown by Figure 4.

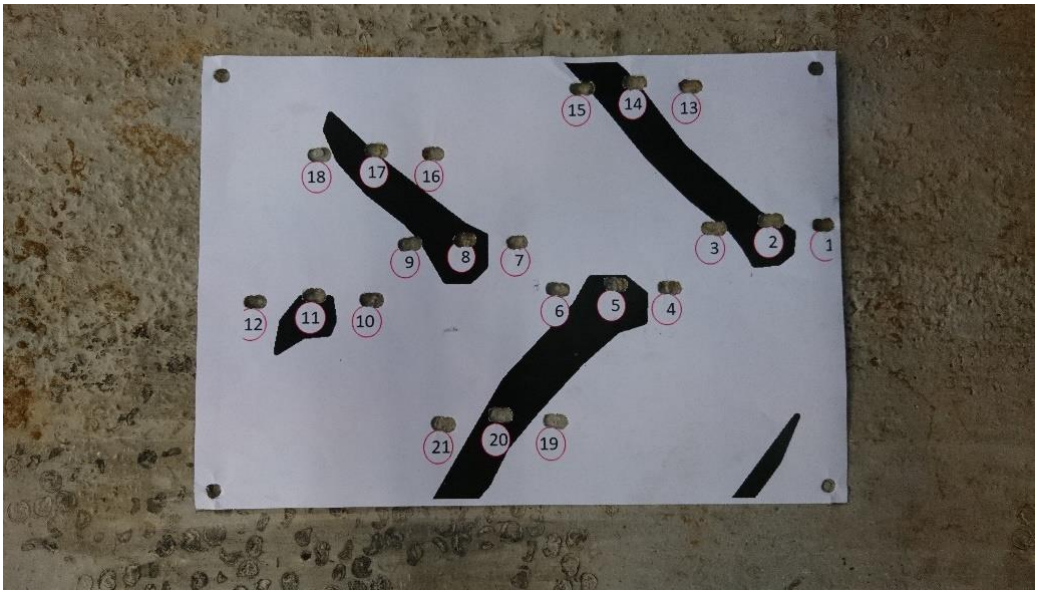

Figure 3:Microtexture profiling location template.

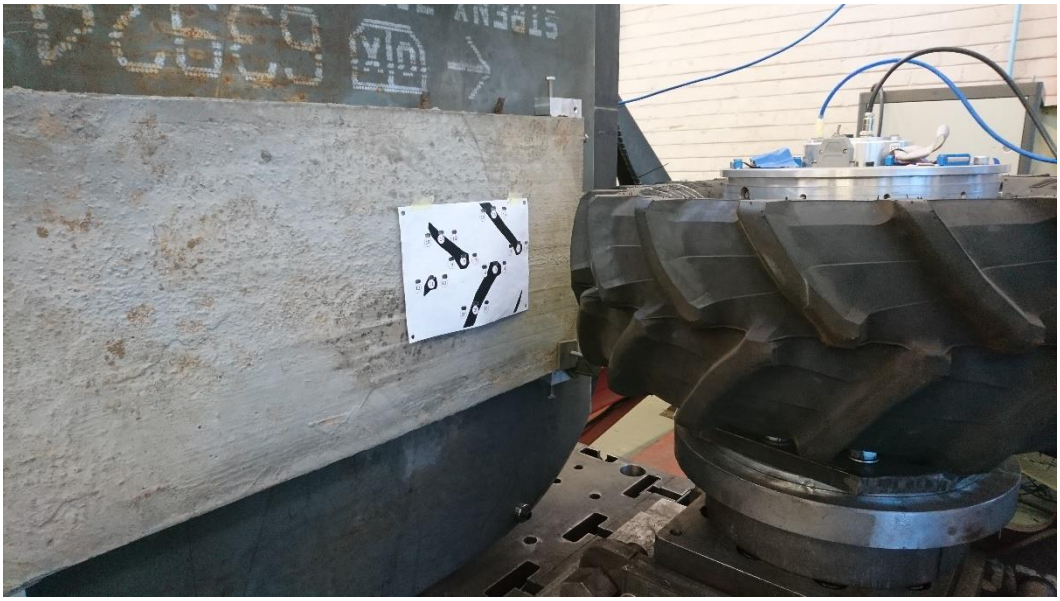

Figure 4: Microtexture profiling location template on STTR fitted with concrete test surface.

The longitudinal friction coefficient was determined on multiple surfaces in a laboratory and on multiple surfaces at the outdoor test track, Gerotek Test Facilities. The list of test surfaces used is highlighted in bold in Table 1, with the average of the 21 measurements within the contact patch noted. The Mild Steel sheet (construction steel, 300MPa yield strength), Aluminium 6 Series sheet (240-270MPa yield strength) and Strenx Steel sheet (supplied by SSAB, a Nordic and US-based steel company, with 700MPa yield strength) are standard off the shelf materials available in South Africa. The only preparation done on these test surfaces was sanding of the Mild Steel sheet with P80 grit sandpaper (to remove mill slag), all other surfaces were used as delivered from the supplier. All surfaces were cleaned with acetone to ensure that the surface was clean and oil free.

The microtexture surface roughness measurement of sample surfaces are shown in Table 1. The roughness of a surface with a profile sample length (l) can be specified using several parameters ranging from the average roughness (R_a), the maximum peak height (R_p), the mean square value

(R_q), the maximum profile valley depth (R_v), the maximum height (R_z), etc. as described in the International Organization for Standardization ISO 4287-1997 and shown in Figure 5. On closer inspection the microtexture surface roughness measurement values on the test surfaces can vary by up to 98% when compared to the surface roughness of the Klingspor CS 308 Y P80 grit sandpaper.

Table 1: Microtexture Surface Roughness Measurements

Roughness Measurements	Condition Standard =ISO 4287:1997 Filter=GAUSS Lc=0.8mm Ls=2.5µm N=5 Pre_Length=OFF Speed=0.5mm/s Range=AUTO Average Pitch=0.5µm		
Surface measured	**R_a [µm]**	**R_q [µm]**	**R_z[µm]**
Mitutoyo Calibration Surface	**2.94**	**3.275**	**10.079**
Cell phone screen protector	0.009	0.012	0.087
Glass	0.014	0.018	0.128
Aluminium 6 Series sheet	0.493	0.6	2.602
Mild Steel_P80 conditioned	1.05	1.251	5.797
Mild Steel sheet	1.227	1.607	7.397
Shaved Tyre	1.293	1.71	8.019
New Tyre	2.58-2.71	3.17-3.45	14-17
paper	2.843	3.382	15.027
Strenx steel sheet	3.06	3.835	17.177
Concrete block STTR	4.983	6.329	27.077
Gerotek High speed concrete track	7.404	8.801	41.508
Asphalt	8-12	10-14	41-51
Used Tyre	10.343	12.895	54.391
New tyre post P80 test	10.782	13.074	50.899
Gerotek concrete	11.367	14.289	64.743
P180 grit sandpaper VSM RK700X	11.526	15.361	71.739
TM700 buffed tyre	11.853	14.671	59.57
P220 grit sandpaper Klingspor CS311Y	14.607	17.486	70.330
Belgian block	15.148	18.234	72.397
P180 grit sandpaper Klingspor CS311Y	18.245	21.988	88.167
P120 grit sandpaper	18.906	23.174	85.028
P100 grit sandpaper	26.209	31.717	123.52
P80 grit sandpaper Klingspor CS308Y	27.772	33.019	118.66

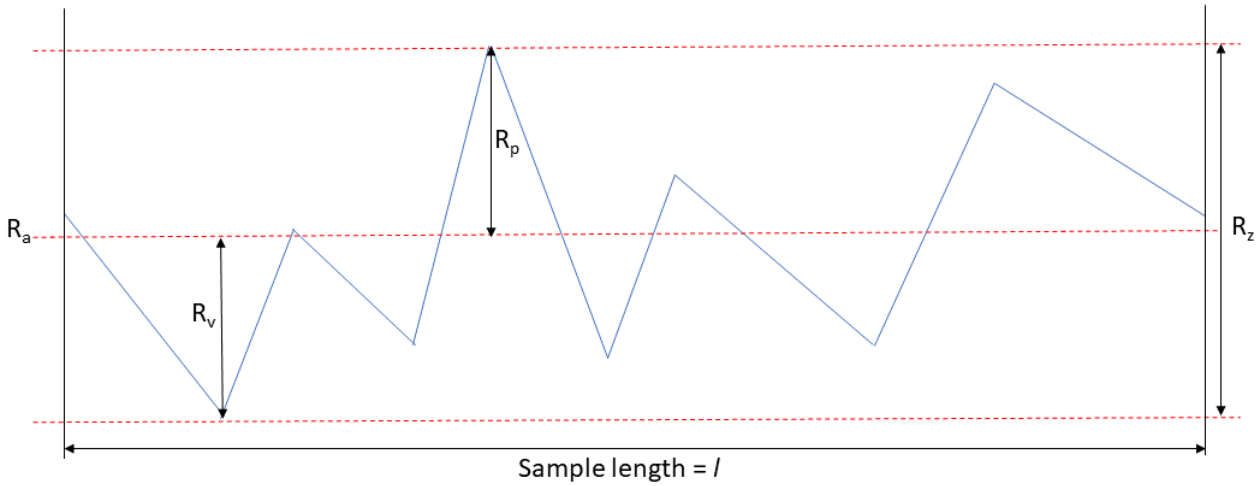

Figure 5:Surface roughness parameters.

The microtexture profiles and DSD of some of the surfaces in Table 1 are shown in Figure 6 and Figure 7 respectively. The microtexture surface profiles can give one a visual indication of the roughness of the surface. The black lines in both Figure 6 and Figure 7 are from the calibration surface of the Mitutoyo SJ-210 portable surface roughness tester. The calibration surface profile is a continuous corrugation/sinusoidal waves, with a constant amplitude and wave length of 10µm. This is clearly shown by the black DSD line in Figure 7, as it has a distinct peak at 10^4 cycles/m indicating that the profile is not random. When comparing the DSDs of the other surfaces it is clear that most surfaces have random amplitudes generally following a straight-line trend on a log-log scale.

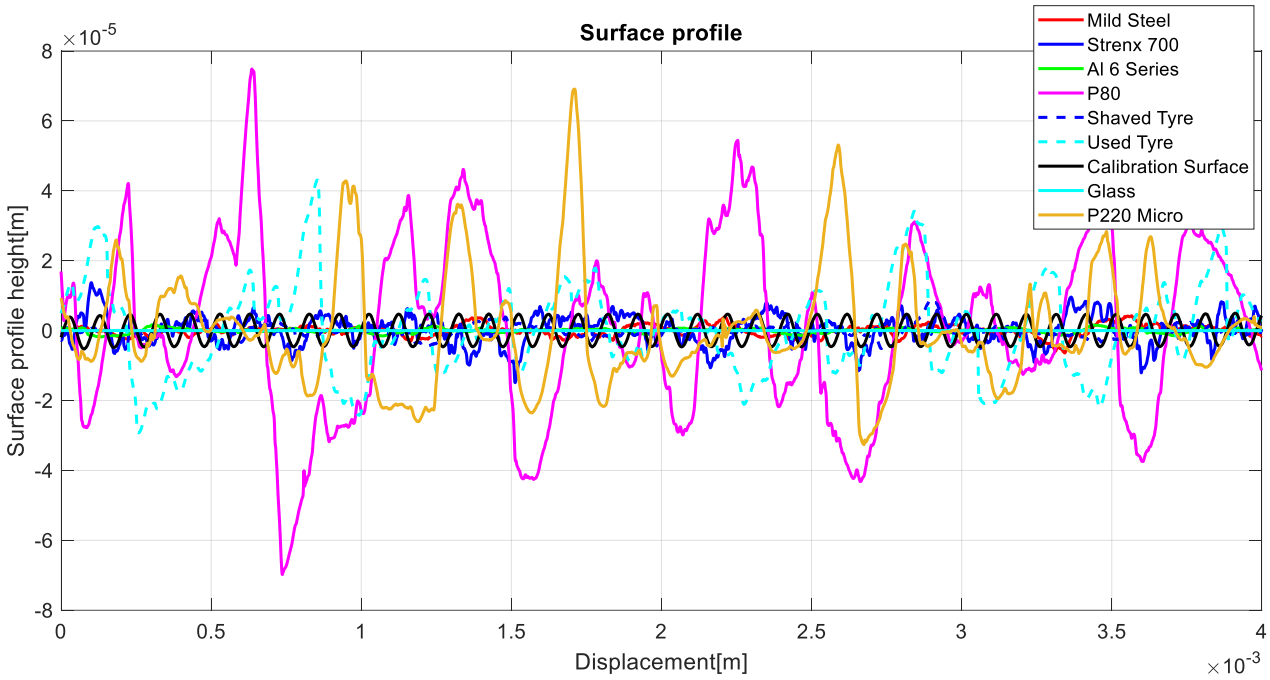

Figure 6: Microtexture profile of sample surfaces.

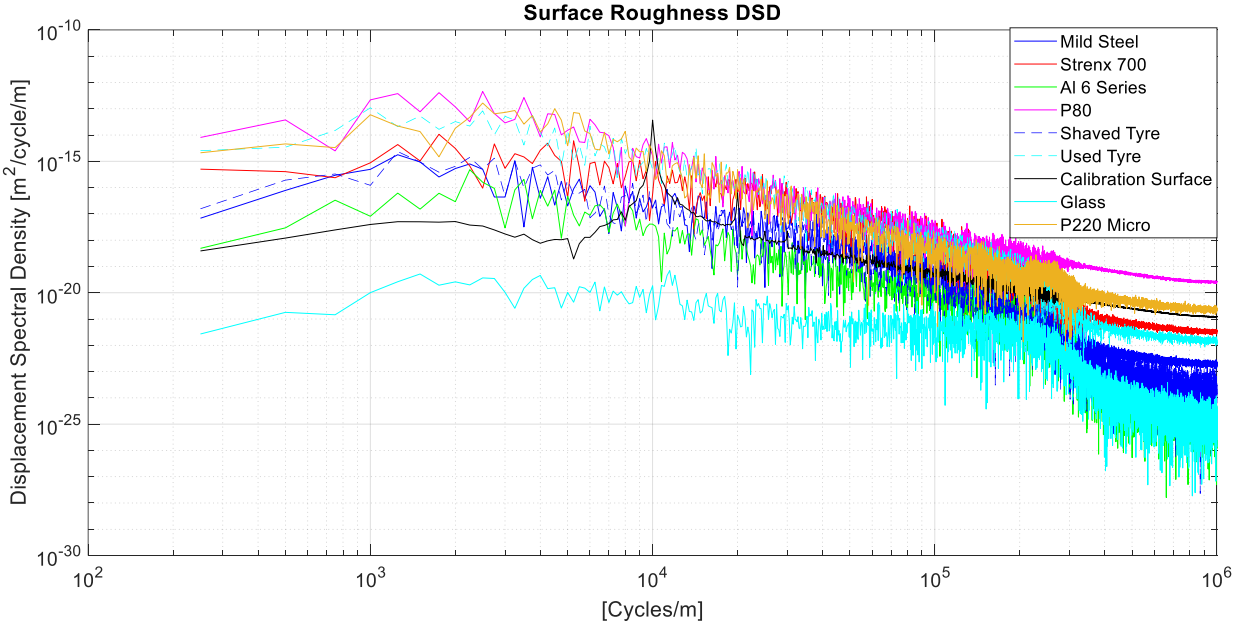

Figure 7: DSD of microtexture profiles of sample surfaces.

Some of the test surface microtexture profiles used on the STTR and at the Gerotek Test Facilities, are presented in Figure 8 with the corresponding DSDs shown in Figure 9. To put the

profiles in perspective, the different road class indicators, as per ISO 8608, are added to the DSD plot in Figure 9, as well as some of the profiles of the concrete tracks and Belgian paving track at the Gerotek Test Facilities as presented by Becker and Els (2014).

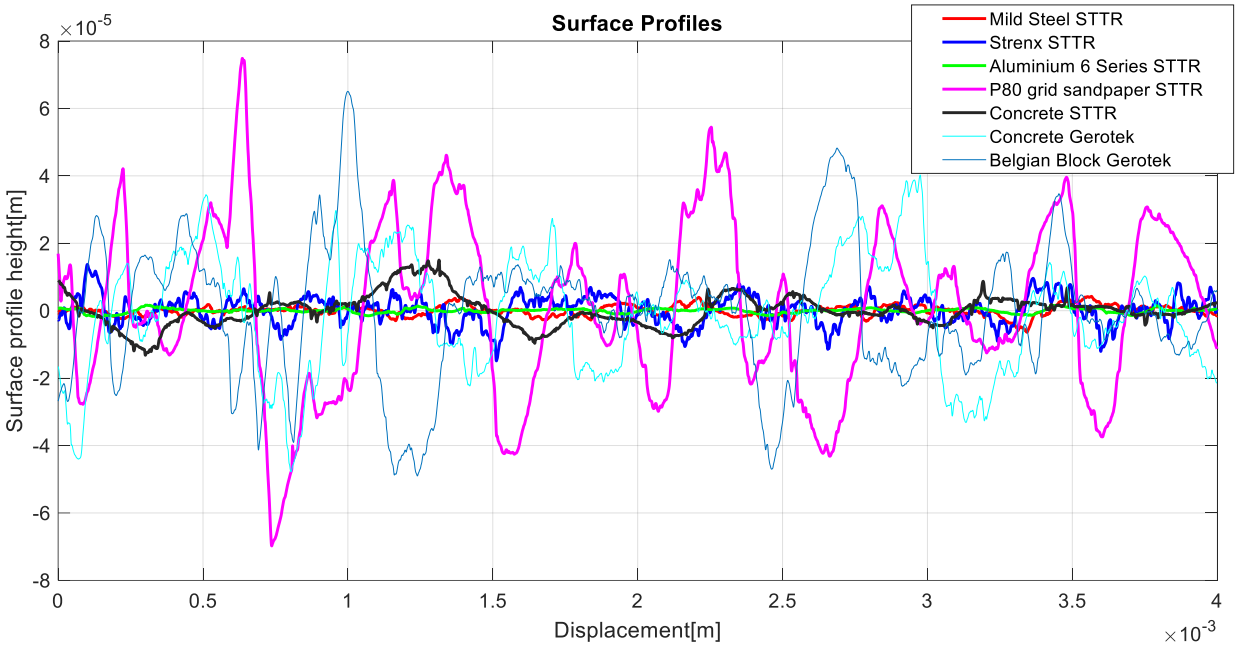

Figure 8:Microtexture profile of test surfaces.

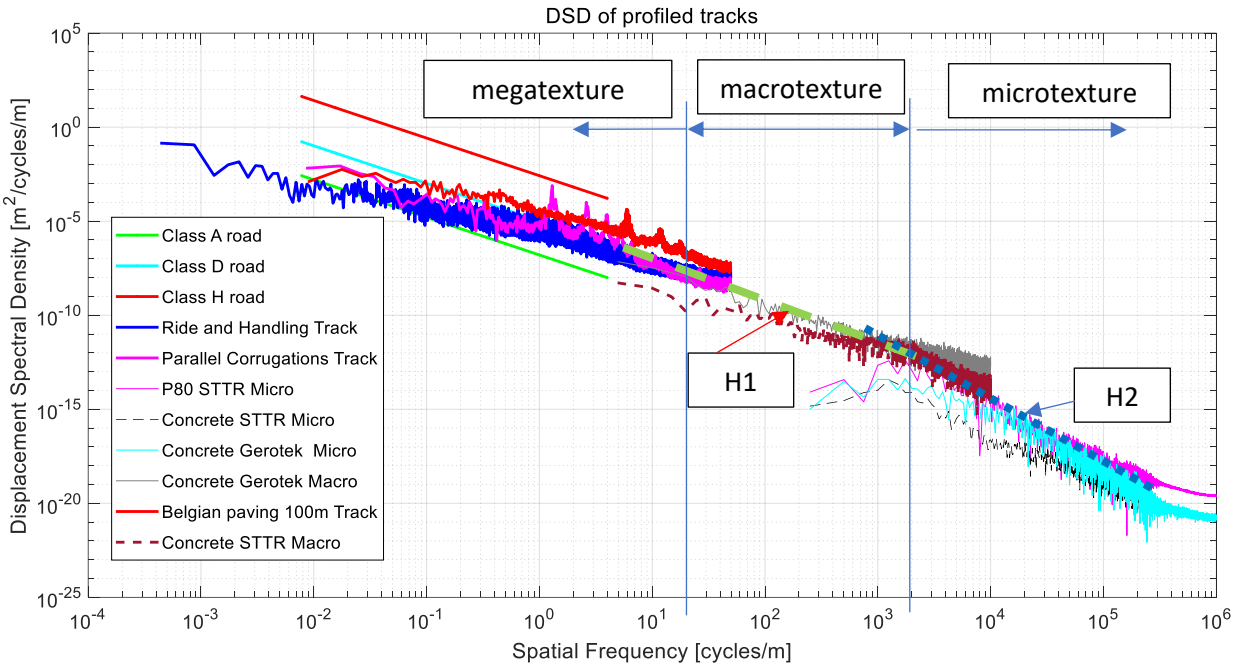

Figure 9: DSD of test surfaces.

It can be seen from Figure 9 that the gradient of the DSD of the mega texture (wavelengths exceeding 50mm, 20cycles/m) measurements on the Gerotek concrete tracks, Ride and Handling track and Parallel Corrugations track, correspond to the macrotexture measurements on the concrete surface as used on the STTR, as shown in Figure 4, between spatial frequencies 10^1 to 10^4 cycles/m. The change in gradient (road index) of the green dashed line, H1, to the blue dotted line, H2, correspond to the Hurst exponent of macro- and microtextures respectively as described by Le Gal et al. (2008). H1 is referred to as the road index where H2 can be described as the surface index.

4. Test Tyre of Interest

More agricultural vehicles are used on asphalt roads as farmers need to travel between fields and move stock around. As a result, designers of agricultural vehicles need to know how these

agricultural tyres react on non-deformable terrains as it has a direct impact on the driveline of these vehicles. Measuring tyre characteristics on any tyre is not a trivial exercise. The logistics, setup time and costs increase with tyre size. The following section describes the tyre and the equipment used during this study to measure the longitudinal friction coefficient on different surfaces. The tyre of interest for this study is a Trelleborg TM700-280/70R16 agricultural tyre with large lugs, a load index of 112 (1120kg) and speed rating of A8 (40km/h). This tyre was previously used to compare methods for measuring motion resistance (Becker and Els, 2020). The selected tyre reduced the logistics required to conduct the analysis. The results can be used to select a larger tyre to be used for future studies. This current study formed part of the investigation into the agricultural tyre stiffness change as a function of tyre wear (Becker and Els, 2022).

The tyre characteristics in the form of the longitudinal friction coefficient of the tyre on different surfaces for two inflation pressures at 100% tread, 50% tread and 0% tread were determined. The different tread conditions were as follows:

- 100% Tread – New tyre, run-in, static tests conducted post motion resistance tests, (Becker and Els, 2020), where no traction or braking was applied to the tyre. Tread depth at 30mm.
- 50% Tread – 15mm of tread shaved with tyre regrooving tool with surface buffed post shaving.
- 0% Tread – Additional 15mm of tread shaved and tyre buffed post shaving.

Figure 10 shows the condition of the tyres used during this study.

Figure 10:a)Trelleborg TM700-280/70R16 tyre with 100% tread, b) Trelleborg TM700-280/70R16 tyre with 50% and 0% tread respectively.

5. Contact Area and Contact Pressures

The size of the tyre contact patch has a direct impact on the longitudinal and lateral force generated by the tyre as this represents the amount of rubber in contact with the non-deformable terrain. The contact patch was captured by painting the tyre and applying the 5.68kN vertical load. For this purpose, a sheet of white paper was used between the tyre and a smooth steel test surface on the STTR for each inflation pressure and tread wear condition. The footprints for each tread wear condition at 80kPa and 200kPa are shown in Figure 11, with the red line a reference indicator of 10mm x 100mm. The thin dashed line shows the change in contact patch perimeter between tread conditions. The contact area was determined by taking the sum of the black paint print within the perimeter of the footprint.

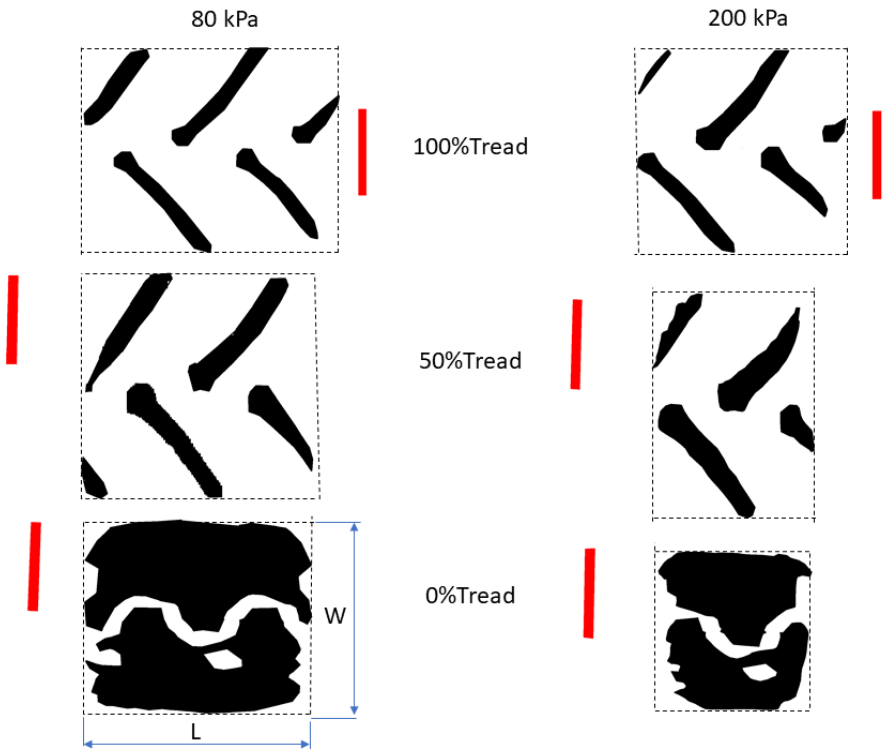

Figure 11: Footprints at different tread conditions and two inflation pressures, with the red block a 10x100mm scale.

The pressure distribution of the three tread conditions at 200kPa was measured with the use of a TireScan system from Tekscan (2021), connected to an 8001-pressure sensor, mounted on the STTR. The three pressure maps for an inflation pressure of 200kPa are shown in Figure 12 with blue indicating low pressure, green – medium pressure and red - high pressure.

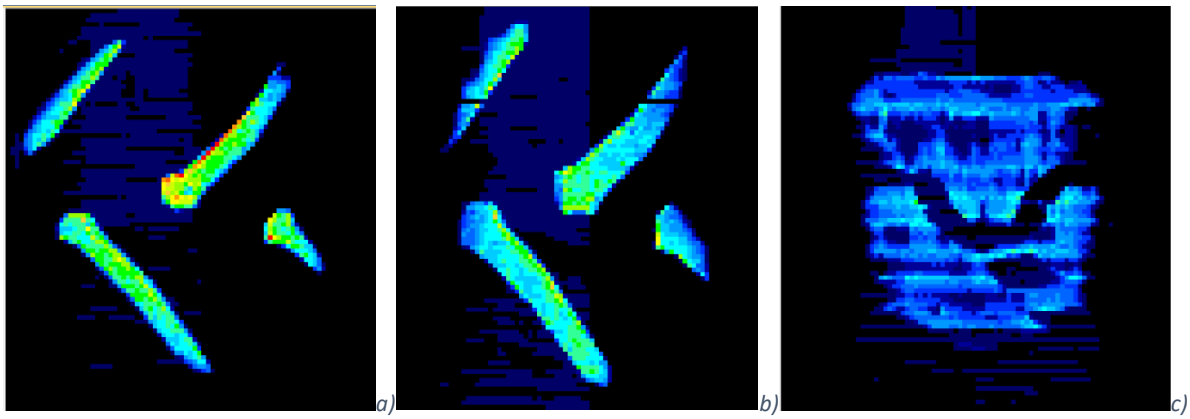

Figure 12:TM700-280/70R16 Pressure distribution at 200kPa for a)100% Tread, b) 50% Tread and c) 0% Tread, respectively.

From the footprints and pressure maps it is noticed that the 100% tread condition has a longer footprint compared to the 50% tread condition which has an overall wider footprint and wider tread blocks. The wider tread blocks are due to the taper shape of the tread block. The 0% tread condition has the smallest perimeter measurements; however, this condition has the highest rubber contact areas of the three conditions, thus it has the lowest contact pressure. The change in pressure was estimated with the use of eq.(6).

$$\text{Pressure} = \frac{\text{Force}}{\text{Area}} \qquad \text{eq. (6)}$$

The average contact pressure in the footprint due to the change in footprint size/tread wear condition is presented in Table 2, along with the area of actual rubber in contact area and the perimeter of the contact patch.

Table 2: Estimated average contact pressure as a function of tread wear and inflation pressure, with rubber in contact area and perimeter dimensions.

Tread wear condition	Constant vertical load of 5.68kN					
	200kPa	**80kPa**	**200kPa**	**80kPa**	**200kPa**	**80kPa**
	Average contact pressure [kPa]		**Rubber in Contact Area [mm^2]**		**Perimeter of Contact Patch, L x W [mm]**	
100% tread	669	476	8490	11909	240x235	300x240
50% Tread	657	492	8642	11534	180x250	265x250
0% Tread	270	157	21021	35993	165x180	265x220

It can be seen in that the contact pressure slightly increases at the lower inflation pressure of 80kPa as the tread wears from 100% to 50%. A 60 to 66% contact pressure drop is noted at 0% tread condition due the increase in actual rubber in contact with the test surface. The contact area for 0% tread condition and an inflation pressure of 80kPa, increases by 202% compared to the 100% tread condition at 80kPa. The contact area for 0% tread condition for an inflation pressure of 200kPa increase by 147% compared to the 100% tread condition at 200kPa. The effect of inflation pressure and tread wear on contact area and contact pressure is highly significant.

6. Laboratory and Outdoor Test Equipment

Physics based tyre models, in the form of FTire, use static tyre parameters to generate the tyre model and uses the dynamic tests to validate the tyre model. The static characterisation of large tyres can be beneficial as dynamic tyre test rigs for tyres with vertical load ratings above 5 000kg are not available due to the large power requirements to test these tyres. The longitudinal stiffness characterisation setup on the STTR is shown in Figure 13 with a) the Klingspor CS 311 Y P80 grit sandpaper surface fitted and b) Belgian Paving block fitted to the STTR. The surface in the red dashed square can be changed to a different surface with ease. Longitudinal characterisation tests are conducted by loading the tyre with a normal load of 5.68kN, followed by a longitudinal displacement of the road plate at 8mm/s.

a)

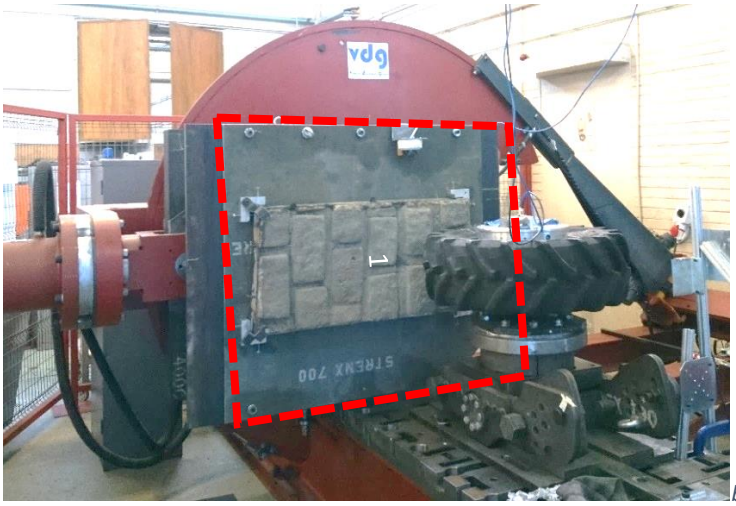

b)

Figure 13:Static Tyre Test Rig from the Vehicle Dynamics Group at the University of Pretoria fitted with a) P80 grit sandpaper and b) Belgian paving block

Static/Non-rolling tyre outdoor tests, used to determine the outdoor longitudinal friction coefficient, conducted at the Gerotek Test Facilities, with the use of the Damping Test Trailer (DTT) from VDG, as shown in Figure 14. The DTT has no suspension fitted and is loaded with ballast weights to have a vertical load of 5.68kN per wheel. In general, the DTT is used for tyre damping measurements. The DTT has the capability to lock the wheels to ensure 100% longitudinal slip during the static longitudinal stiffness tests. The tests are conducted with the brakes on the trailer applied. The tow vehicle pulls the trailer as slow as possible in a straight line for up to 150mm longitudinal displacement. During this longitudinal displacement of the non-

rolling tyre, the tyre deforms and the longitudinal and normal load on the tyre is measured with the use of Wheel Force Transducers. With these forces known the longitudinal stiffness and sliding friction coefficient can be calculated and compared with the results from the laboratory tests on the STTR. Due to the ambient temperature of 25 degrees Celsius and slow longitudinal test velocity, in the order of 8mm/s, the flash temperature and change in temperature of the rubber in the contact patch was deemed insignificant and was not taken into consideration.

Figure 14: Damping Test Trailer from the Vehicle Dynamics Group at the University of Pretoria fitted with TM700-280/70R16 tyres.

Dynamic/Rolling tyre outdoor tests, were conducted at the Gerotek Test Facilities, with the use of the Dynamic Tyre Test Trailer, as shown in Figure 15. The test procedure involves three different approaches to determine the longitudinal and lateral forces, and the force envelope (or friction circle) at 100% tread condition. The longitudinal force test procedure involves accelerating the DTTT up to the desired constant speed. The brake pressure on the measurement axle is then gradually increased. The brake application rate is adjusted for each test setup, as it is dependent on

the test speed, applied vertical load and brake temperature. When the highest possible longitudinal load is reached or the wheels lock, the brakes are released and the wheels are allowed to accelerate back up to the free-rolling speed. The procedure is repeated several times during the same test run. The lateral force test procedure involves accelerating the DTTT up to speed and then changing the tyre slip angles on the measurement axle continuously, sweeping from -1° slip to 18° slip at a constant rate. The force envelope tests involve changing the slip angle in discrete increments with the actuators and increasing the brake pressure until the maximum longitudinal load is reached while the slip angle is maintained constant. The brake pressure is in turn released and the slip angle is changed to the next increment. The brake pressure is increased again and the process repeats up to the maximum lateral slip angle. Tests can be conducted at camber angles from -5 to 5 degrees in 1-degree increments. Test speeds of up to 80km/h can be achieved, but speeds are usually kept low due to excessive tyre wear and heat build-up during testing at high speeds. On large off-road and agricultural tyres, the test speeds are limited by the tyre's speed rating.

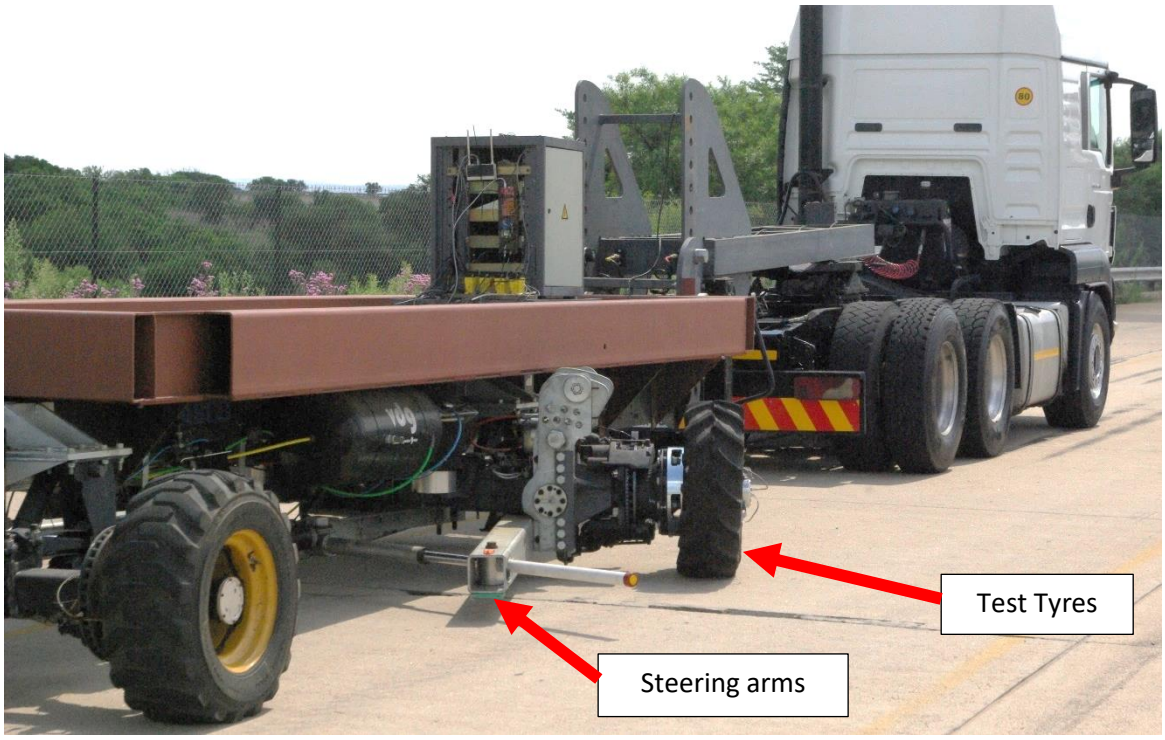

Figure 15: Dynamic Tyre Test Trailer from the Vehicle Dynamics Group at the University of Pretoria testing with TM700-280/70R16 tyres.

7. Test Results

The following sections describe the tyre characteristics of a static/non-rolling tyre and dynamic/rolling tyre respectively followed by comparing static test results with dynamic test results.

7.1 Static/Non-Rolling Tyre Characterisation on Multiple Surfaces

The typical spread of longitudinal friction coefficient measurements is shown in Figure 16 for the same test conducted on the same tyre with different surfaces in a laboratory with the use of the STTR at the two inflation pressures. All the measured data was left unfiltered to ensure all the

surface roughness effects are kept in the data sets and not filtered out. It is clear that the longitudinal stiffness of the tyre is captured well by using any of the surfaces, however the maximum longitudinal friction coefficient generated by the tyre varies significantly. This is a direct result of different surface roughness for each of these test surfaces. Persson (2001), confirmed that the friction of rubber on smooth surfaces are due to interfacial adhesion and has the largest effect for surfaces with a surface roughness value Ra<1µm. When Ra.> 1µm the adhesion should have little to no effect on the friction coefficient.

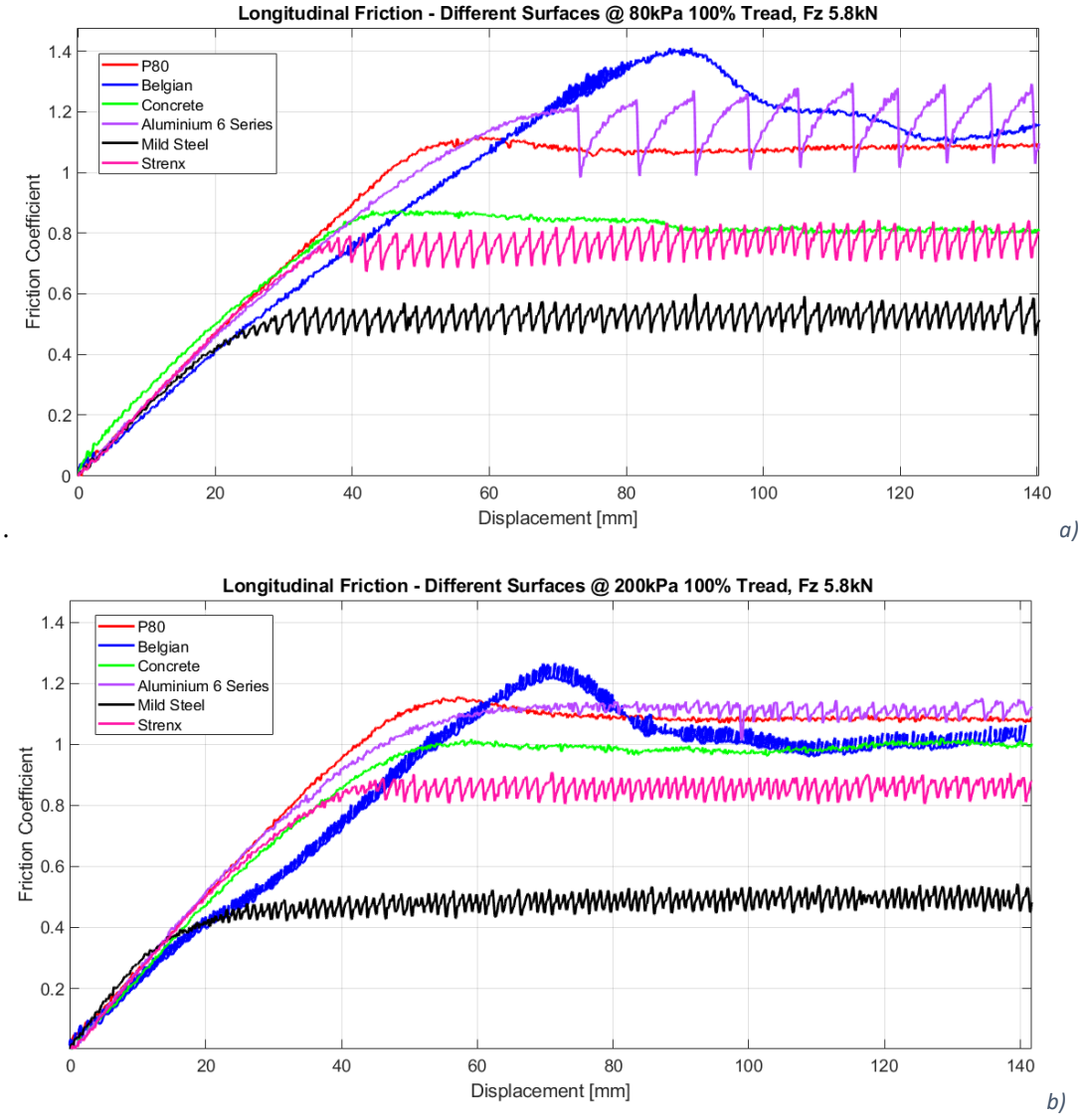

Figure 16:Longitudinal friction coefficient measurements on different surfaces for a) 80kPa and b) 200kPa inflation pressure, respectively.

Figure 16 illustrates the contribution of the adhesion, as the measured friction coefficient on the Alumunium sheet, with a surface roughness of R_a=0.493µm, is larger than 1. In comparison to, the Mild Steel sheet which has a significantly lower friction coefficient of 0.5 with a higher surface roughness of R_a=1.227µm. Note the "sawtooth" response in Figure 16. This stick-slip phenomina will be disccused later. The measured DSD of the microtexture on test surfaces are shown in Figure

7. The DSD of the Alumimium sheet and Mild Steel sheet differs only at the higher spatial frequencies > 10^5 cycle/m. This is where the adhesion contribution is the highest as the DSD of the Aluminium sheet is lower. It can be seen that the concrete surfaces is in mid-range when compare to the DSD of P80 sandpaper and Mild Steel sheets. From these graphs it can be seen that the higher the DSD the higher the measured friction coefficient, with the exception of the Mild Steel and Aluminium sheets.

The main focus of this study is to compare laboratory tests to outdoor test at a single vertical load on the tyre. Additional tests were conducted to illustrate how tyre characteristics change with different vertical loads as shown in Figure 17. This is an important aspect to consider when conducting vehicle simulations at vertical tyre loads for which the tyre models were not validated. This supports the argument that it is very important to validated the tyre model for the application it will be used for and that large simulation errors will be made if a tyre model is used outside the validation scope. The longitudinal stiffness of a tyre can vary by 64% and the sliding friction coefficient can vary by 10% on the same surface and the same tyre tread wear condition.

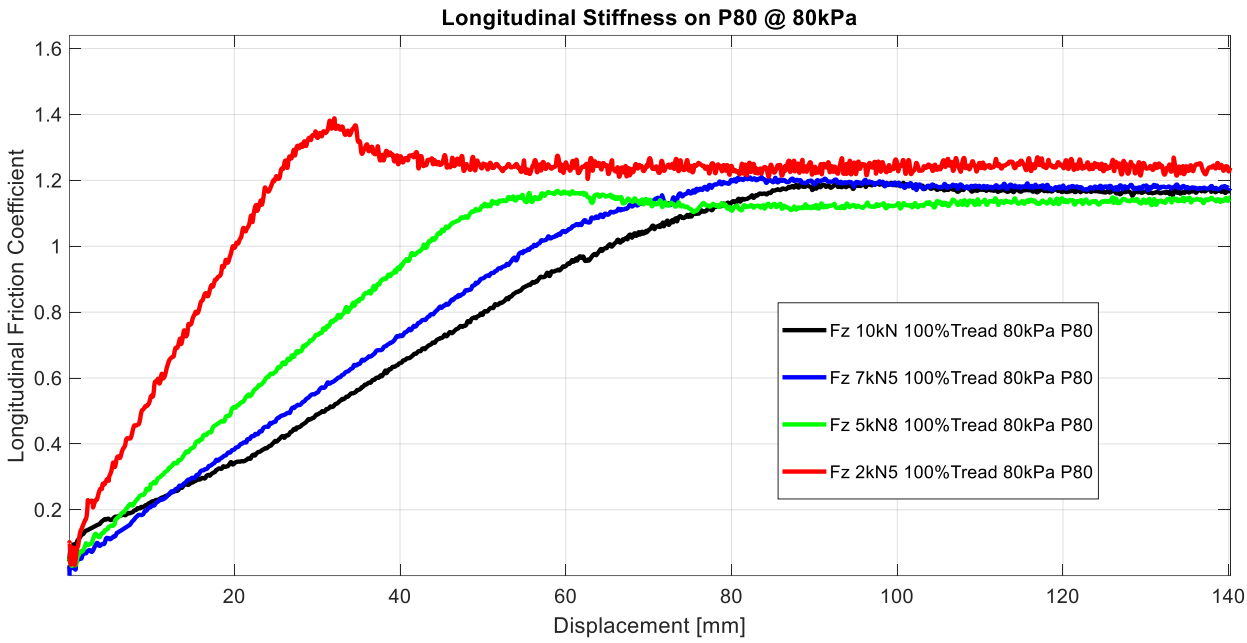

Figure 17:Longitudinal friction coefficient at multiple normal loads for 200kPa inflation pressure and 100% tread condition.

The same variation in longitudinal stiffness is noticed when the vertical load is varied and the tread wear condition is kept constant at 50% tread wear at a lower inflation pressure, as shown in Figure 18.

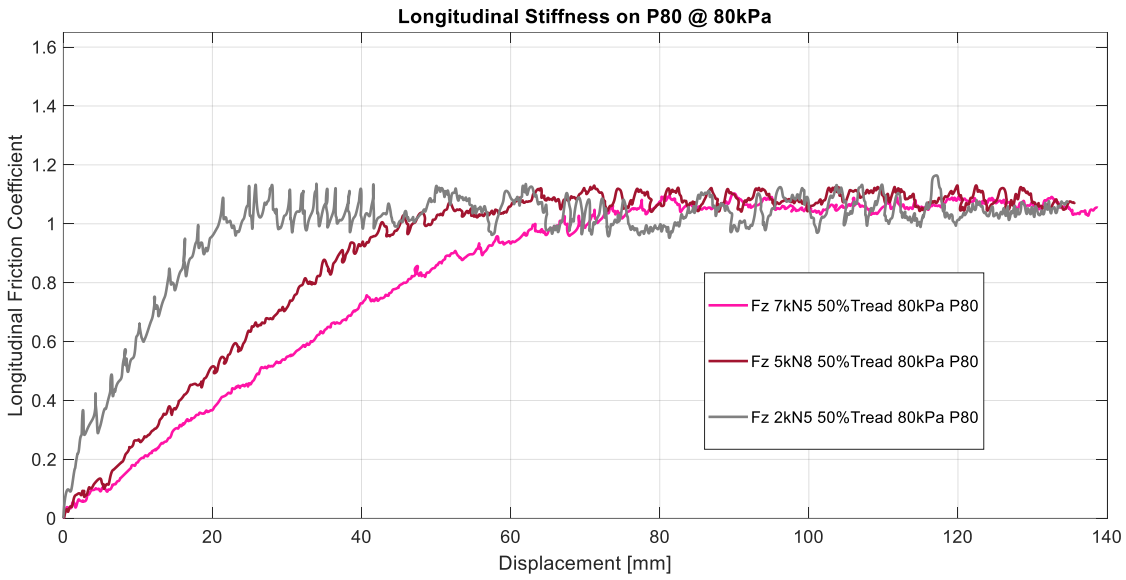

Figure 18:Longitudinal friction coefficient at multiple normal loads for 80kPa inflation pressure and 50% tread condition

When the vertical load, surface roughness and inflation pressure is kept constant, the effect of the tread on the longitudinal stiffness and friction coefficient becomes apparent as shown in Figure 19. From Figure 19 it is clear that the tread wear condition has less than 10% variation on the longitudinal stiffness and friction coefficient when the tread condition is 50% to 100%. The higher longitudinal stiffness at 0% tread condition is due to the removal of the deformation of lugs in the tread, thus only the inflated carcass stiffness is measured which is 21% higher. This indicates that the lugs decrease the longitudinal stiffness of the tyre. The large change of 50% in friction coefficient between 50% tread to 0% tread, is due to the significant increase in the actual amount of rubber in contact with the test surface (in the order of 200% increase in rubber contact), as shown in Figure 11 and summarised in Table 2, respectively.

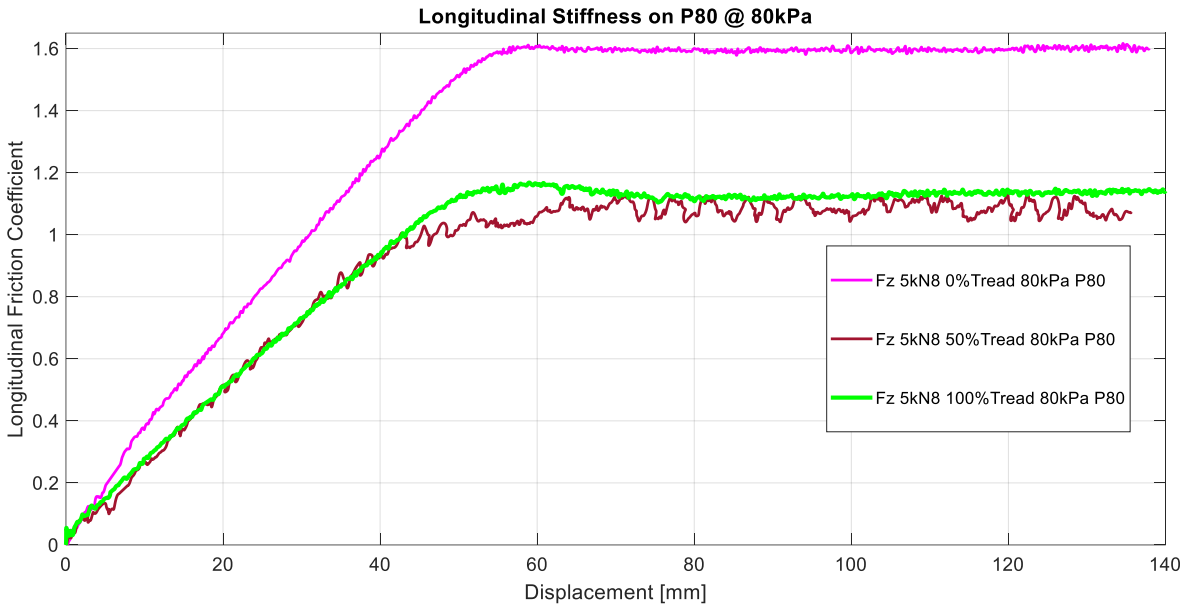

Figure 19: Longitudinal friction coefficient at constant load and inflation pressure with change in tread condition.

Due to the size and shape of the lug in the tread, for the agricultural tyre of interest, one can simplify the bending/deformation of the lug to a cantilever beam with the longitudinal force applied at the tip of the lug in the contact patch as shown in Figure 20.

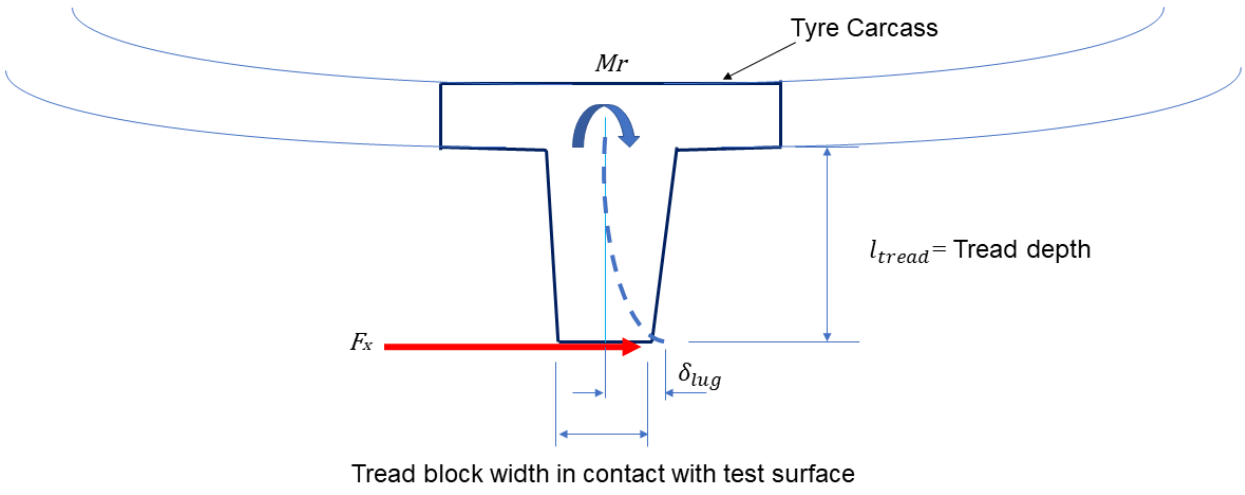

Figure 20: Longitudinal deformation of tread lug simplified to a cantilever beam.

The deformation of the lug can thus be described by eq. (7) which is the calculated bending of a cantilever beam, as presented by Shigley (1986),

$$\delta_{lug} = \frac{F_x * l_{tread}^3}{3EI_{lug}} \qquad \text{eq. (7)}$$

The displacement, δ_{lug}, is directly proportional to the height cubed of the tread, l_{lug}. In this case the hight of the tread block, is 30mm at 100% tread and 15mm at 50% tread. The reactive bending moment, M_r , at the clamped side of the beam (the tyre carcass and belt) is related to the inflation pressure as the belt and carcass stifness is strongly dependent on the inflation pressure. This reactive bending moment needs to counter the bending moment generated by the longitudinal force which is proportional to the height of the lug as shown in eq. (8):

$$M_r = F_x l_{tread} \text{ eq. (8)}$$

The longitudinal deformation of the lugs in the tyre tread is shown in Figure 21 for 100% tread and 50% tread, respectively, at an inflation pressure of 80kPa. The stick-slip that is seen on multiple smooth surfaces at only 100% tread condition, as shown in Figure 16, is due to the longitudinal deformation and the bending stiffness of the lugs. At 100% tread condition the lug deforms and increases the applied bending moment on the tyre carcass. The reactive bending moment in the tyre belt, supplied by the inflation pressure in the carcass, is just not enough to counter the applied bending moment. As a result the lug deforms more and as soon as the leading edge detaches from the surface a detachment wave is produced which propagates from the front-end to the back-end of the contact area. This results in the stick-splip phenomena. At some point,

as the lugs wear down, the applied bending moment becomes lower than the bending moment supplied by the tyre carcass, which in turn holds the deformed lug in position and prevents the detachment waves from forming.

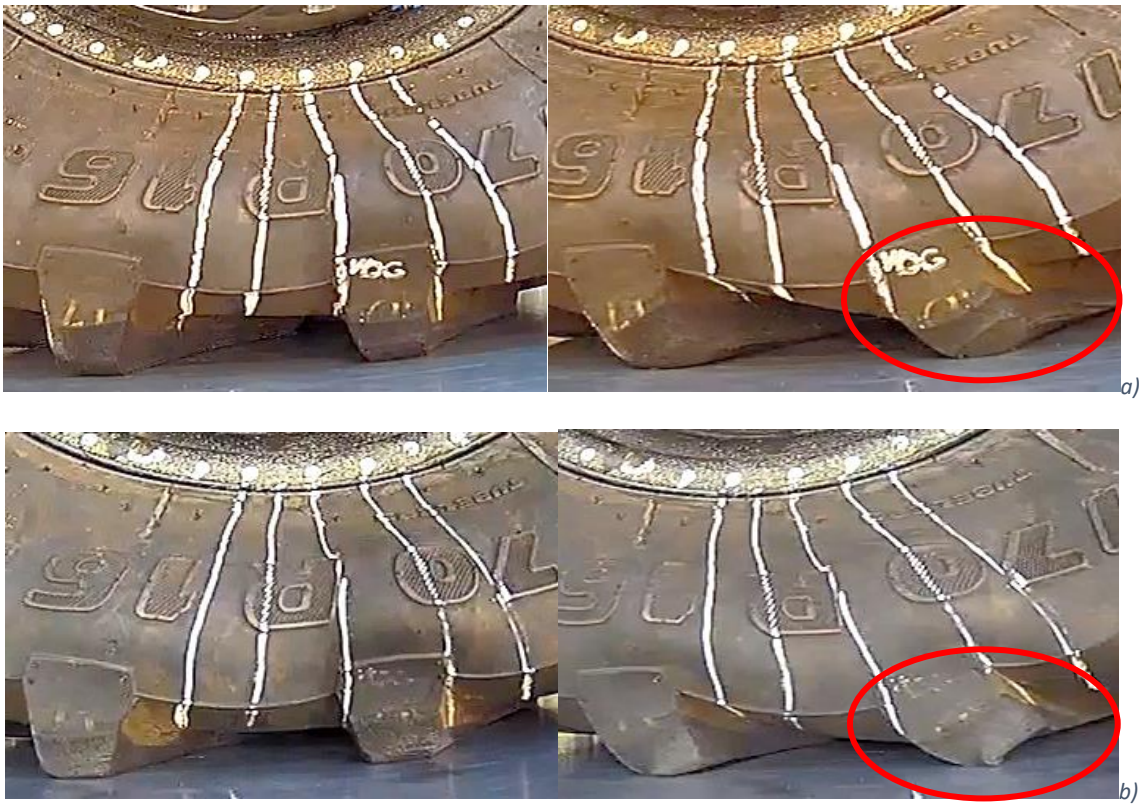

Figure 21:Longitudinal deformation of the tread lugs at 80kPa inflation pressure on an Aluminium sheet at a) 100% tread and b) 50% tread.

Stick-slip theory is described as a mechanical system with a spring damper, where the damper element is linear and the friction force is decsribed by the Stribeck curve which is a discontinuous non-linear function, (Zuleeg, 2015). This mechanical stick-slip mechanism shows that, for a lower tangentional stiffness in the carcass, the displacement oscilation frequency is high. When the carcass stiffness increases, as the inflation pressure is increased, the force displacement oscilations

will be smaller, as shown in Figure 22. A very high friction coefficient is measured on the Aluminium sheet, with surface roughness R_a<1µm, where the adhesion component is very high. A slight change is seen in stick-slip frequency for surfaces with surface roughness values higher than R_a>1µm (Mild Steel and Strenx surface). Note that as soon as the tread condition changes from 100%, no stick-slip is observed in the data. The stick-slip is not noticed during the tests conducted on concrete as shown in Figure 23, even at 100% tread, as the surface roughness of the concrete is higher compared to the surfaces in Figure 22. This is a motivation for using a more representative rough surface during laboratory tests.

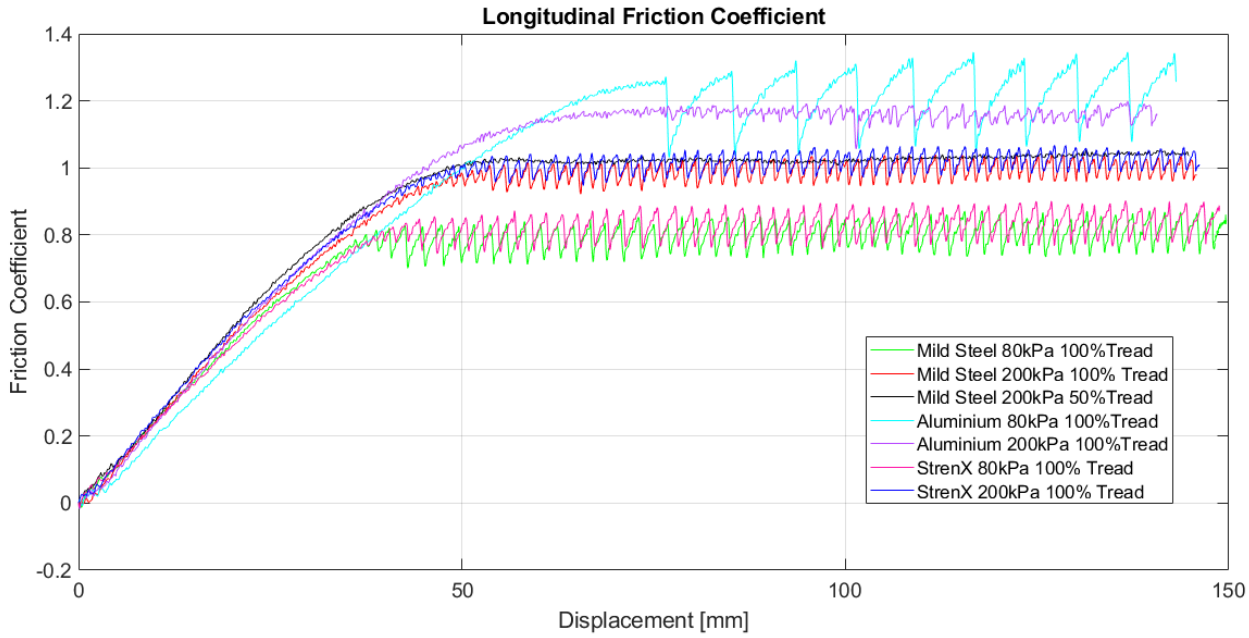

Figure 22:Stick-slip phenomena at different inflation pressures, on variety of surfaces at only 100% tread.

Figure 23 shows the different friction coefficients measured between the laboratory tests on the STTR fitted with a concrete surface and outdoor tests at Gerotek on concrete. The sliding friction coefficient measured during the laboratory tests indicated that the friction coefficient increases in the order of 10% between different tyre tread conditions due to the increase of rubber in the contact

patch, where as the outdoor tests measured a more consistent sliding friction coefficient. It is suspected that this is due to the different ways in which the tyre is constrained between test methods. An average of 13% difference in sliding friction coefficent measurement was noted were as the peak friction was within 3% to 5%. From these results, good correlation is observed between the laboratory tests on the concrete surface, as shown in Figure 4 and outdoor test results as conducted with the DTT on the concrete tracks at the Gerotek Test Facilities (Figure 14). This surface can thus be used with confidence on the STTR to obtain accurate friction coefficient estimates for a tyre and will result in accurate model validated results on the concrete tracks at the Gerotek Test Facilities.

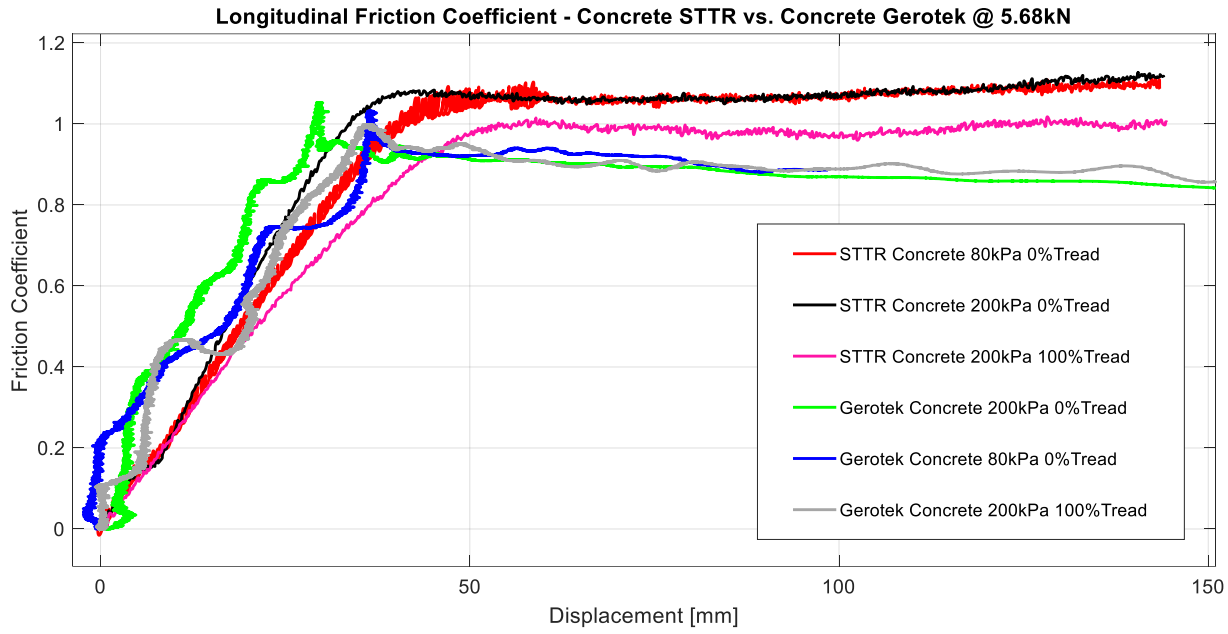

Figure 23: Friction coefficient measurement on concrete in laboratory tests and outdoor tests.

It is noted that the friction coefficient is lower at a higher inflation pressure over the Belgian paving, as shown in Figure 24. The friction coefficient increases due to lug contact at the 100%

tread condition as the lugs slide into the cavities between the bricks in Belgian paving, this also excites the vertical dynamics of the test trailer which cannot happen on the STTR due to the boundary conditions imposed by the test rig. The effect of the gaps between the Belgian blocks on the roughness of the track can also be seen in the DSD of the 100m Belgian profile in Figure 9, where the size of the bricks and gaps are represented by the peaks in the graph. To eliminate the effect of the lugs on the measurements, the friction coefficient at the 0% tread condition are compared over the Belgian paving for both the STTR and Gerotek measurements. The same percentage difference in maximum sliding friction coefficient is noted between the static laboratory tests and the quasi-static outdoor tests over the same section of the Belgian paving surface. The oscillations in the outdoor tests are caused by the different boundary conditions on the tyre during the tests. For the outdoor tests the tyre can move vertically, compared to the STTR where the tyre is constraint in the vertical direction. In general the STTR and Gerotek test results correlate well when considering the different boundary conditions.

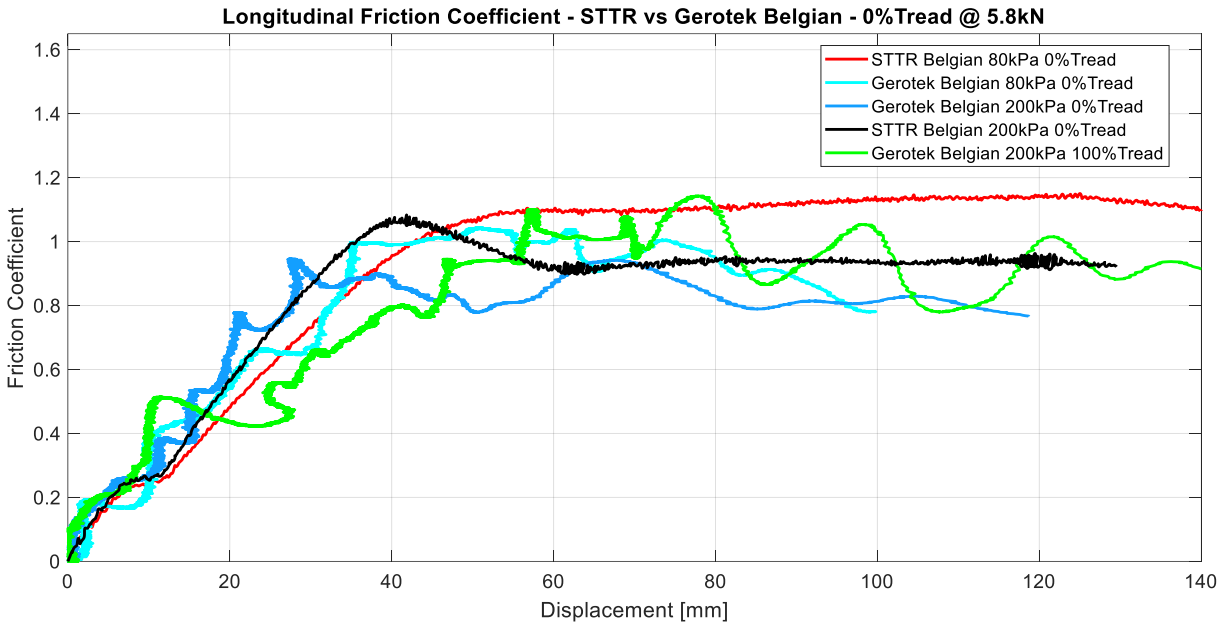

Figure 24: Belgian paving friction coefficient measurements in laboratory tests and outdoor tests.

The change in longitudinal stiffness due to a lower inflation pressure and change in tread wear condition relative to a new tyre at 100% tread inflated to 200kPa, on concrete, is shown in Figure 25. This figure indicates that the roughness of the test surface can have an increasing or decreasing effect on the measured longitudinal stiffness. Only the Mild Steel surface gave a consistent increase in longitudinal stiffness over the range of inflation and tread wear changes. Notice again the large jump when 0% tread is reached. If the 0% tread points are ignored, the longitudinal stiffness is reasonably independent of the surface roughness. This accentuates the complex interaction between the tyre carcass stiffness and friction coefficients.

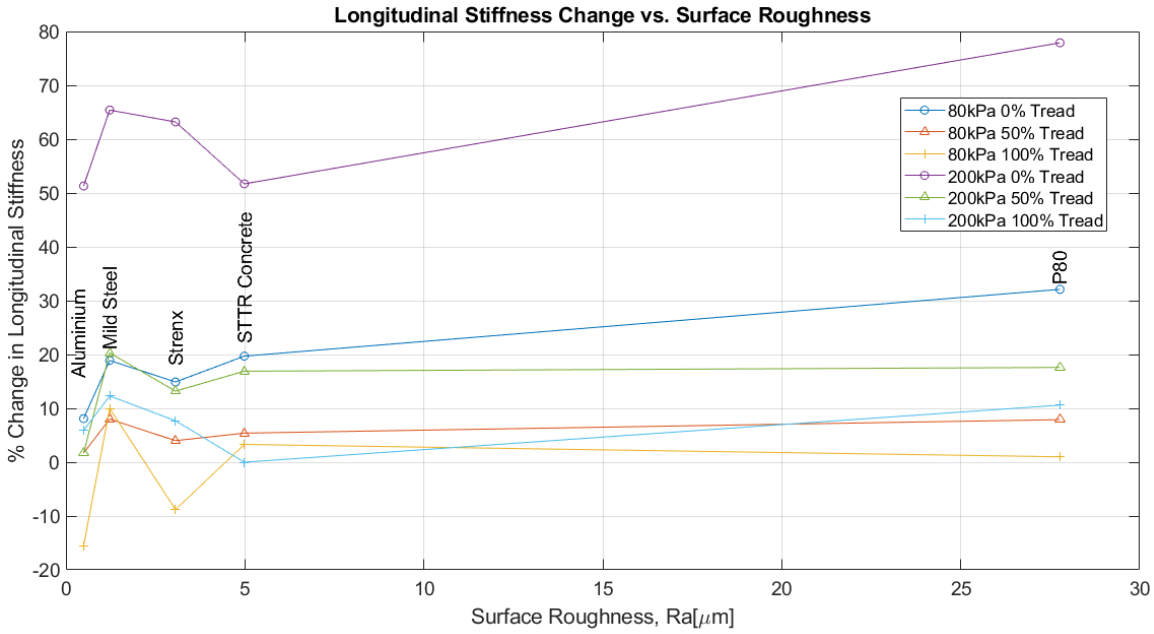

Figure 25:Change in longitudinal stiffness as a function of surface roughness, relative to 200kPa inflated tyre at 100% tread.

Figure 26 shows the effect of the surface roughness on the friction coefficient generated between the rubber and surfaces at different tread wear conditions. This shows that, in general, on very smooth or very rough surfaces one will measure a higher friction coefficient when testing tyres. This figure also shows that when testing on surfaces with $7\mu m<R_a<20\mu m$ a variation in friction coefficient in the order of 20%, for different tread wear conditions on the tyre, can be expected.

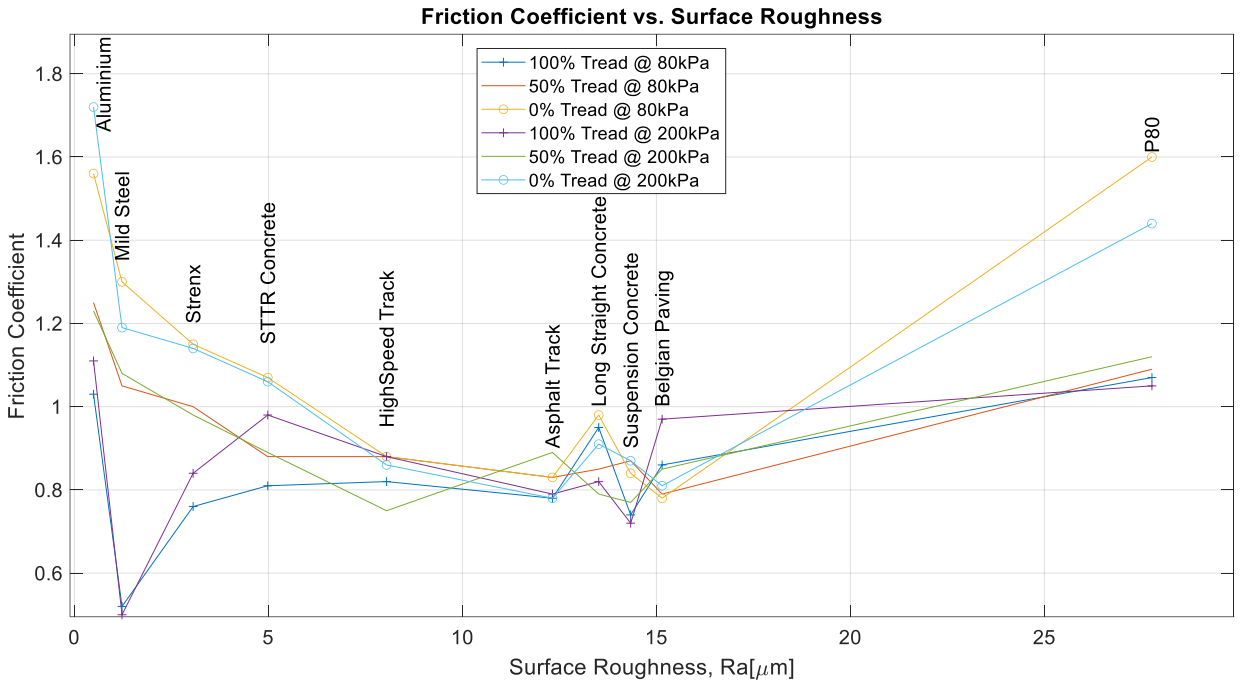

Figure 26: Friction coefficient vs. surface roughness for 80kPa and 200kPa inflation pressure at different tread conditions.

On agricultural tyres the amount of rubber in contact with un-deformable terrain in the contact patch can be a little as 15%, as shown in Figure 11. Figure 27 shows the friction coefficient as function of the surface roughness R_a and percentage rubber in contact with the surface in the contact patch. It is observed that a more consistent friction coefficient is obtained on a surface with $7\mu m<R_a<20\ \mu m$ and with a ratio of rubber in contact with un-deformable terrain in the contact patch of larger than 18%. It is clear that smooth surfaces should not be used as it results in a large scatter in friction coefficient values ranging from 0.5 to 1.7. A large scatter in friction coefficient values are also noted for rough surfaces.

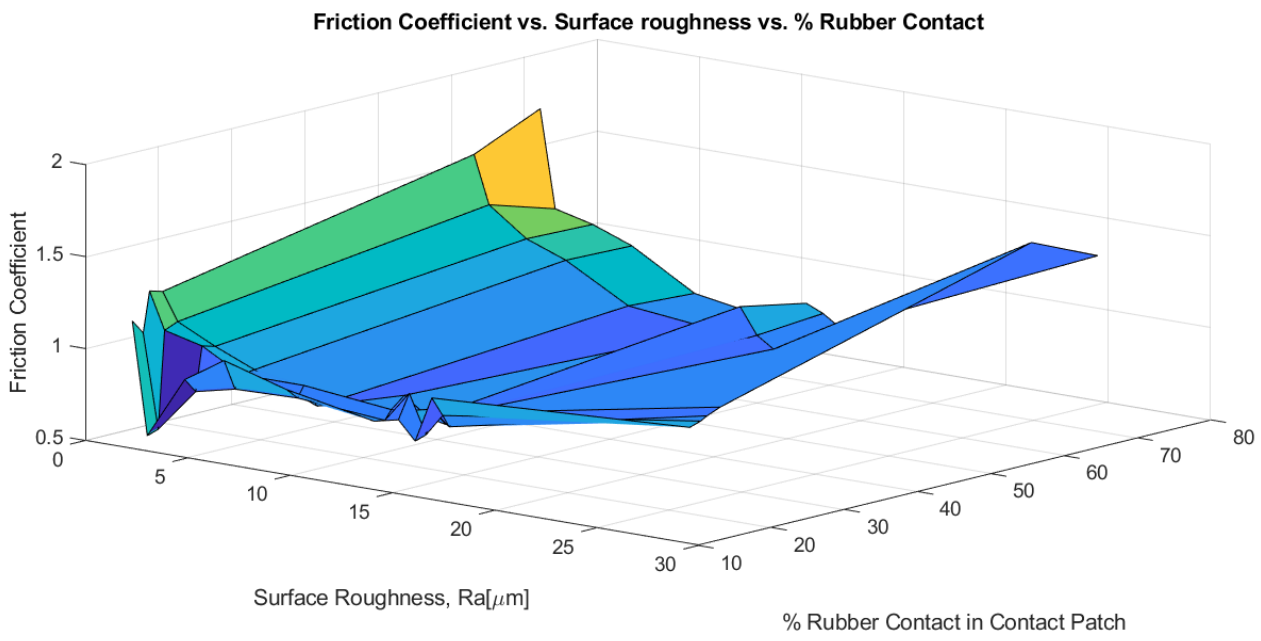

Figure 27:Friction coefficient vs. surface roughness as a function of rubber contact percentage.

This study shows that the surface roughness and DSD should be used to determine which grit sandpaper or corundum tracks need to be used in order to represent the outdoor environment during laboratory tests. It is seen in Figure 26 and Figure 27 that for the concrete outdoor test surfaces at Gerotek, the recommended laboratory test surface needs to have a surface roughness value, $10<R_a<15\mu m$. Table 1 indicated that this roughness is equivalent to a Klingspor CS 311 Y P180 or P220 grit sandpaper. The DSD of P80, P180, P220 grit sandpapers are shown in Figure 28. It can be seen that not all P180 grit sandpapers have the same DSD characteristics. Additional tests on P180 grit RK700X VSM sandpaper resulted in a friction coefficient more representative of the Gerotek concrete surfaces at 0% Tread condition, as shown in Figure 29.

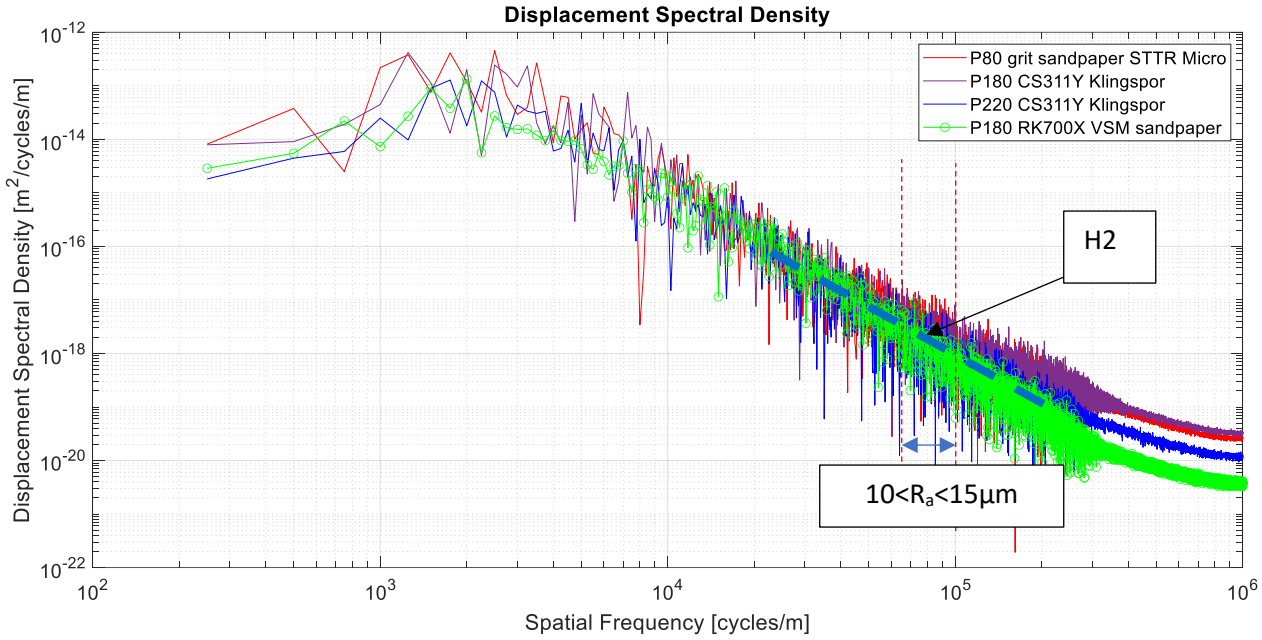

Figure 28: DSD comparison between sandpaper surfaces, with recommended surface index, H2, for laboratory surface to correspond to Gerotek surface.

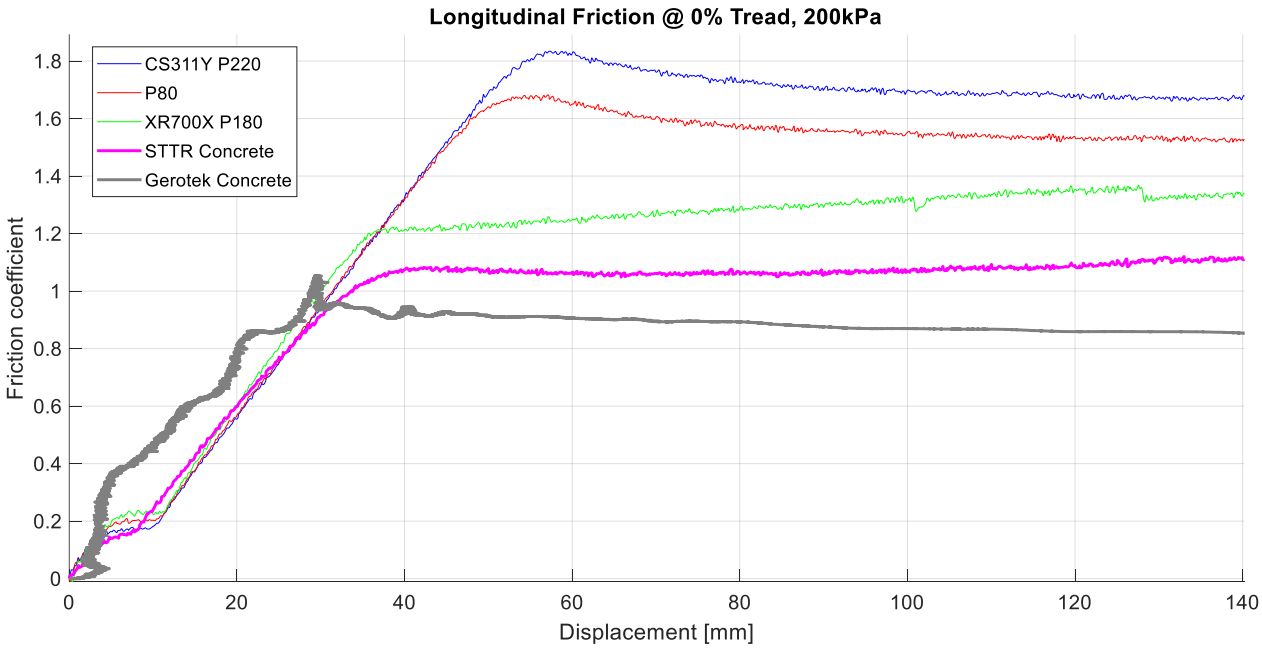

Figure 29:Longitudinal stiffness measurement on different surfaces at 0% Tread.

Figure 29 shows that the P180 grit RK700X VSM sandpaper results in a 32% higher friction coefficient compared to an 80% higher friction coefficient should a P80 grid sandpaper be used. The concrete block used on the STTR was not 100% representative of the Gerotek concrete and resulted in a 17% increase in measured friction coefficient at 0% tread. The surface roughness value of $10<R_a<15\mu m$ correlates directly to the surface texture of the aggregate used in the concrete. This relates to a spatial frequency between 66 666 and 100 000 cycles/m, as indicated in Figure 28, with corresponding surface index, H2, and roughness coefficient at a spatial frequency of 75 000 cycles/m. The majority of the road surface contains exposed aggregate (as shown in Figure 6), which is in direct contact with the rubber in the contact patch, thus the dominating factor in friction generation.

7.2 Dynamic/Rolling Tyre Characterisation on Concrete

Dynamic/rolling tyre characterisation tests were conducted with the use of the DTTT at a vertical load of 5.68kN in order to obtain the longitudinal and lateral characteristics of a tyre, with 100% tread, on concrete.

Unfiltered data for a typical rolling tyre longitudinal friction coefficient vs. longitudinal slip under braking test is shown in Figure 30. The graph shows the longitudinal forces normalized with the vertical force to give the friction coefficient. Instead of only testing at 80kPa and 200kPa inflation pressure as used throughout this study, tests were also performed for inflation pressures of 120kPa and 160kPa. It can be seen that for a rolling tyre, the longitudinal stiffness is very consistent and independent of the inflation pressure at 100% tread condition. This corresponds very well to the

static/non-rolling longitudinal tests conducted on the STTR as shown in Figure 22. Test were conducted at a speed of 11km/h, with a vertical load of 5.68kN, as it is as representative operating speed of the vehicle on which the tyre of interest is typically fitted to.

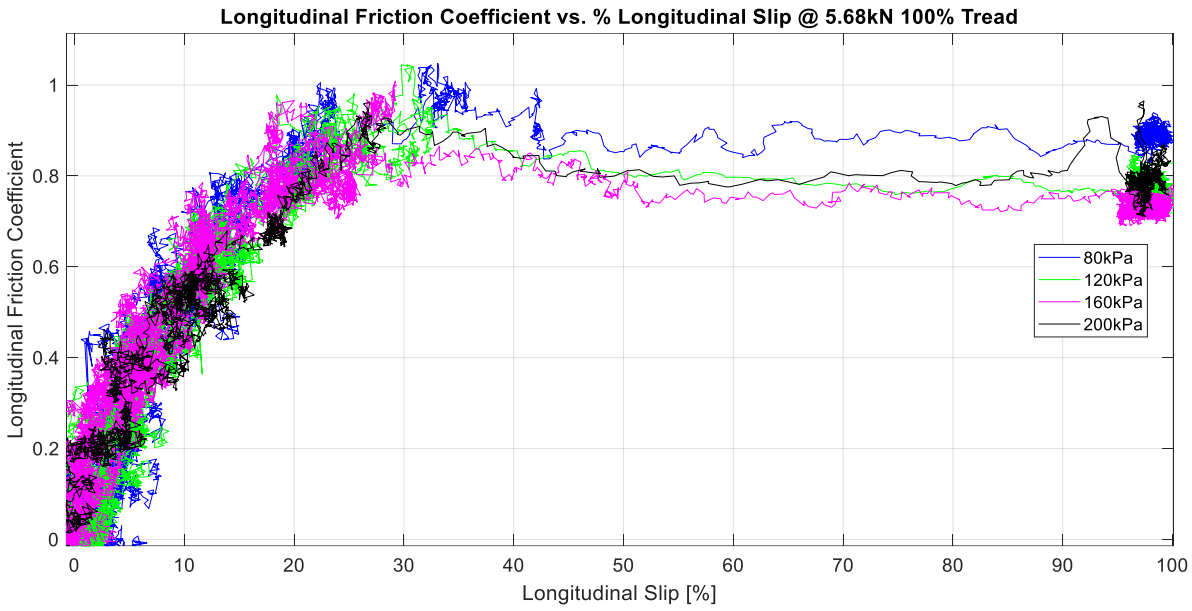

Figure 30: Unfiltered longitudinal friction coefficient vs. longitudinal slip measurements under braking on Trelleborg TM700 280/70R16 at a speed of 11km/h at multiple inflation pressures.

The lateral friction coefficient vs. slip angle of a rolling tyre is as repeatable as the longitudinal test. An example of the unfiltered lateral test data is shown in Figure 31, where it can be seen that the lateral stiffness of the rolling tyre is very consistent and independent of the inflation pressure, which is the opposite than observed for a static/ non-rolling tyre. This is caused by the stiffening of the carcass belt as the tyre rotates. The effect of the lugs in the tread pattern and radial runout are clearly seen in the vertical force oscillations in the data as seen in Figure 31.

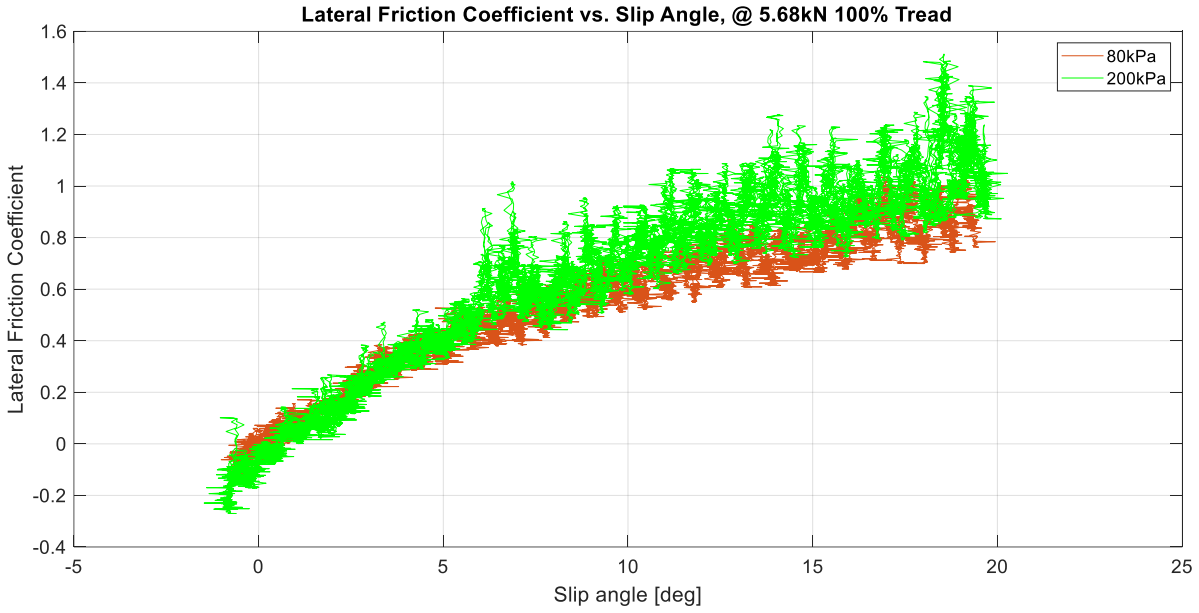

Figure 31: Unfiltered lateral friction coefficient vs slip angle measurements on Trelleborg TM700 280/70R16 at 11km/h, at 80kPa and 200kPa inflation pressure.

During the friction envelop tests the tyre is rolling at a set slip angle with the brakes applied up to wheel lockup. Figure 32 shows the state of the lateral deformation of the tyre before and during lockup. This is a clear representation of why a vehicle, that is operating at the limit, can only generate a maximum steering force or only apply a maximum braking force. The maximum combined forces will always be lower.

Figure 32: Friction envelope tests on Trelleborg TM700 280/70R16 at 11km/h, vertical load at 5.68kN before and during lockup at a constant lateral slip angle, respectively.

The friction envelop describes the combination of the applied longitudinal and lateral forces during different slip angles and longitudinal wheel slip as shown in Figure 33. It can be seen that at 80kPa inflation pressure a larger longitudinal friction coefficient can be generated due to a larger footprint at 80kPa, also noted in Figure 30 during pure longitudinal slip tests. The increased side wall stiffness, due to the increased inflation pressure, correlates to the increase maximum lateral friction coefficient generated at 200kPa.

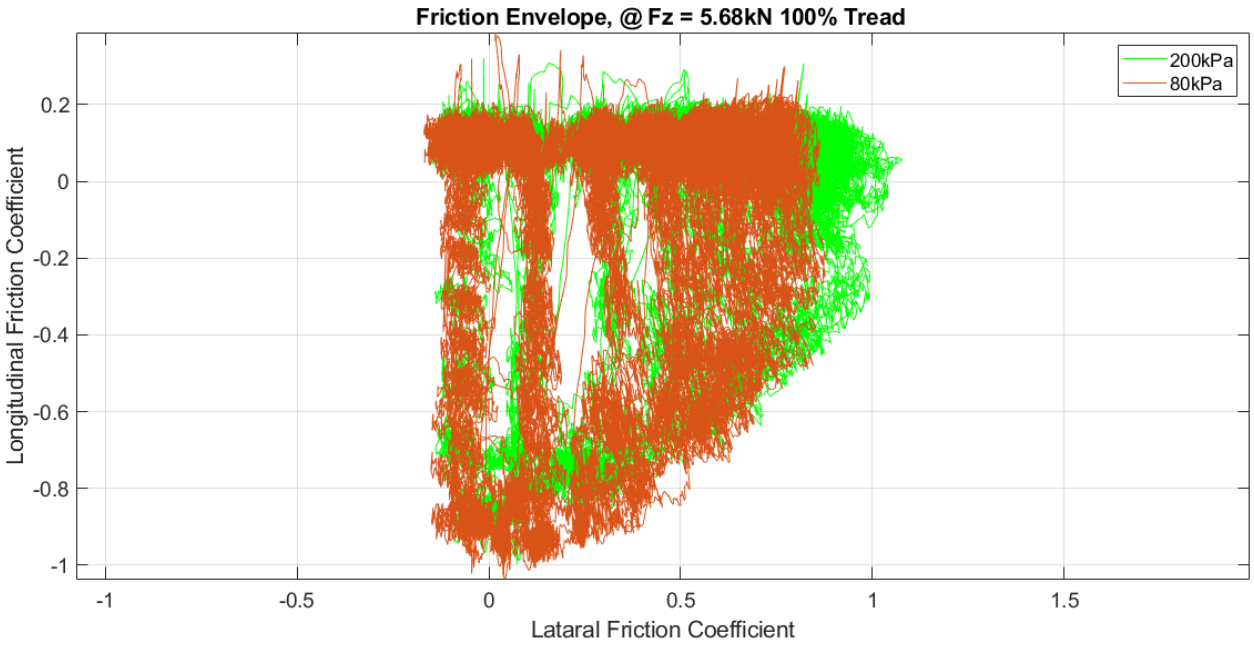

Figure 33: Friction envelop unfiltered measurement on Trelleborg TM700 280/70R16 at 11km/h, at 80kPa and 200kPa inflation pressure, respectively.

7.3 Static/Non-rolling Tyre Characterisation vs. Dynamic/Rolling Tyre Characterisation on Concrete

Outdoor dynamic tyre tests are time consuming, expensive and less repeatable over different times of year testing than tests conducted in a laboratory. Also tyre size/load limitations are a major factor when conducting dynamic/rolling tests on large tyres. If static test rig results could be used to, at least estimate, tyre parameters that represent dynamic/rolling characteristics, it can become more affordable to obtain tyre characteristics in order to parameterize more tyre models. A method to compare the longitudinal friction coefficient as a function of % longitudinal slip of a rolling tyre to static/non-rolling longitudinal friction coefficient as a function of longitudinal displacement, is to translate longitudinal slip of the contact patch to longitudinal displacement, $D_{longStatic}$. For the

dynamic longitudinal slip tests this can be achieved by calculating the longitudinal displacement of the contact patch, D_{wheel}, relative to the displacement of the vehicle ($D_{vehicle}$) and dividing it by the number of wheel rotations, N_{rotate}, during the longitudinal slip period from 0% to 100% slip as shown in eq. (9):

$$D_{longStatic} = \frac{(D_{vehicle} - D_{wheel})}{N_{rotate}} \qquad \text{eq. (9)}$$

The result of this transformation from % longitudinal slip to relative longitudinal displacement is shown in Figure 34.

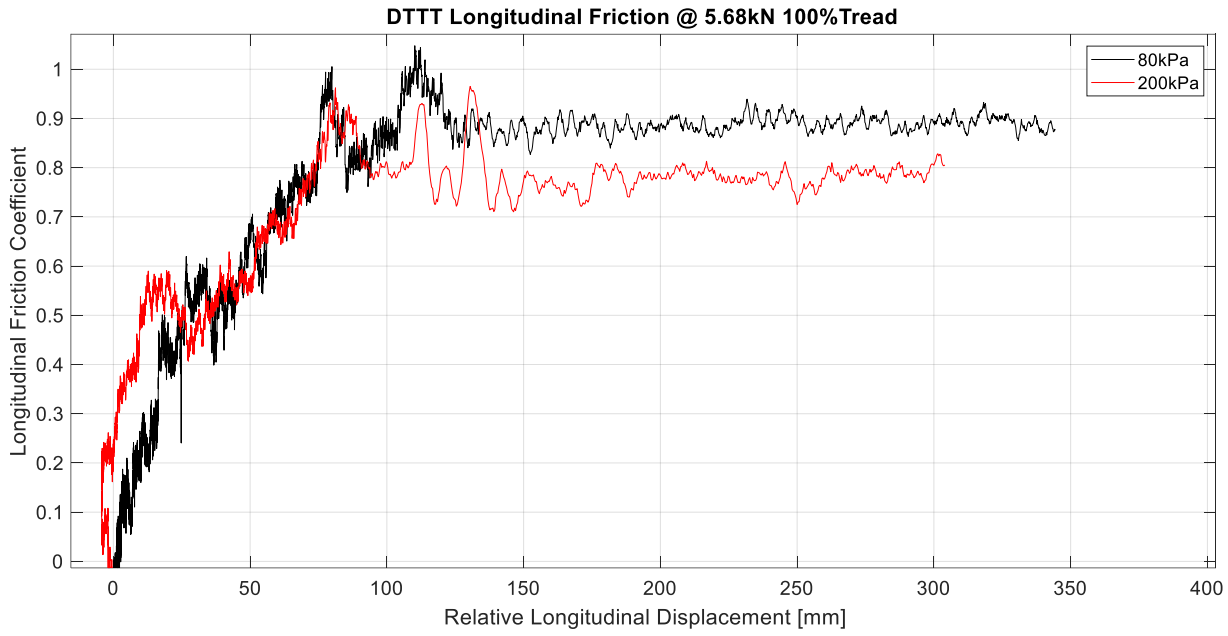

Figure 34: Translated Rolling Longitudinal Friction Coefficient vs. Relative Longitudinal Displacement at 80kPa and 200kPa inflation pressure, respectively.

Figure 35 shows the comparison between the static tests conducted on the STTR on concrete, the DTT static tests at Gerotek and the translated DTTT tests.

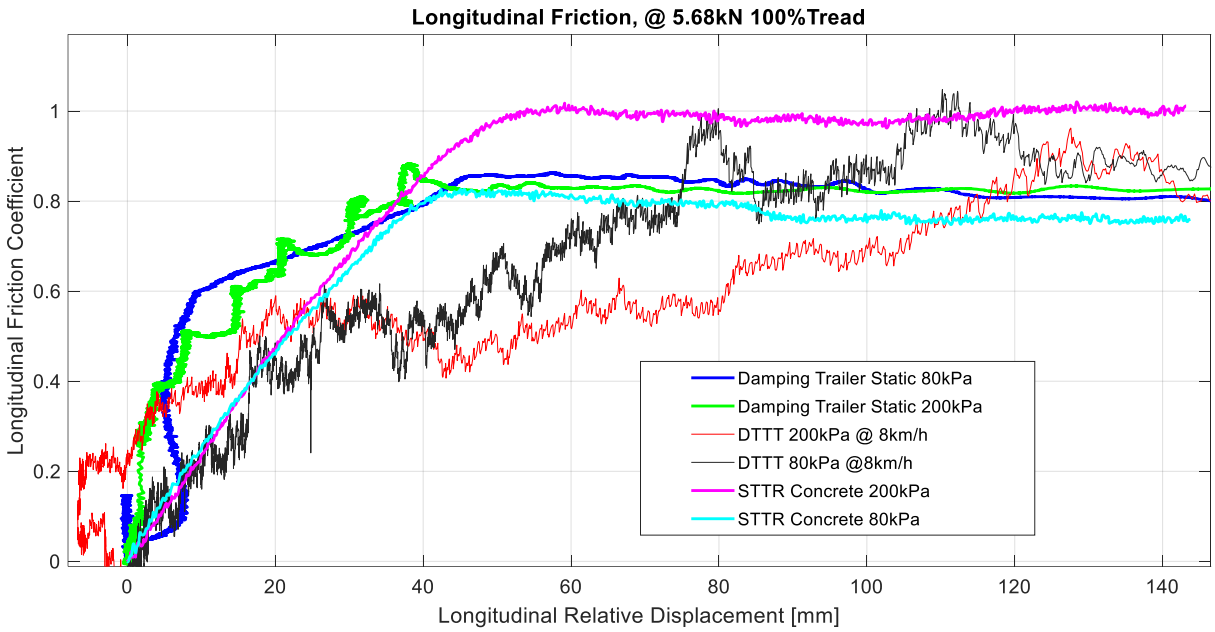

Figure 35: Longitudinal Friction Coefficient vs. Longitudinal Displacement from different test methods.

Relatively good correlation is seen between the three test methods. The initial longitudinal stiffness correlates very well within the first 30mm of longitudinal stiffness, with the maximum sliding friction coefficient within 10 to 20% for the tests conducted on the Gerotek track with the DTTT. The DTT results correlate very well with the STTR results at 80kPa, the difference at 200kPa is due to the difference in boundary conditions.

The lateral friction coefficient vs. slip angle tests can be translated to the lateral friction coefficient vs. 90-degree lateral displacement with the use of trigonometry to calculate the lateral displacement component, $Slip_{Lat\_mm}$, at the specific lateral slip angle, β, and the contact patch length, L, as shown in eq. (10):

$$Slip_{Lat\_mm} = Ltan\beta \qquad \text{eq. (10)}$$

As seen in Figure 36, the lower inflation pressure does not correlate very well due to the stiffening of the belt when the tyre rotates. The belt stiffening has the largest effect on the lateral force generated at lower inflation pressures. The result of the comparison between the static tests on the STTR on concrete with the lateral translation of the friction envelope tests and lateral force vs. slip angle tests at 200kPa inflation pressure with 100% tread is shown in Figure 37. Very good correlation is seen at the high inflation pressure tests. This shows consistency for all three tests methods being static or dynamic.

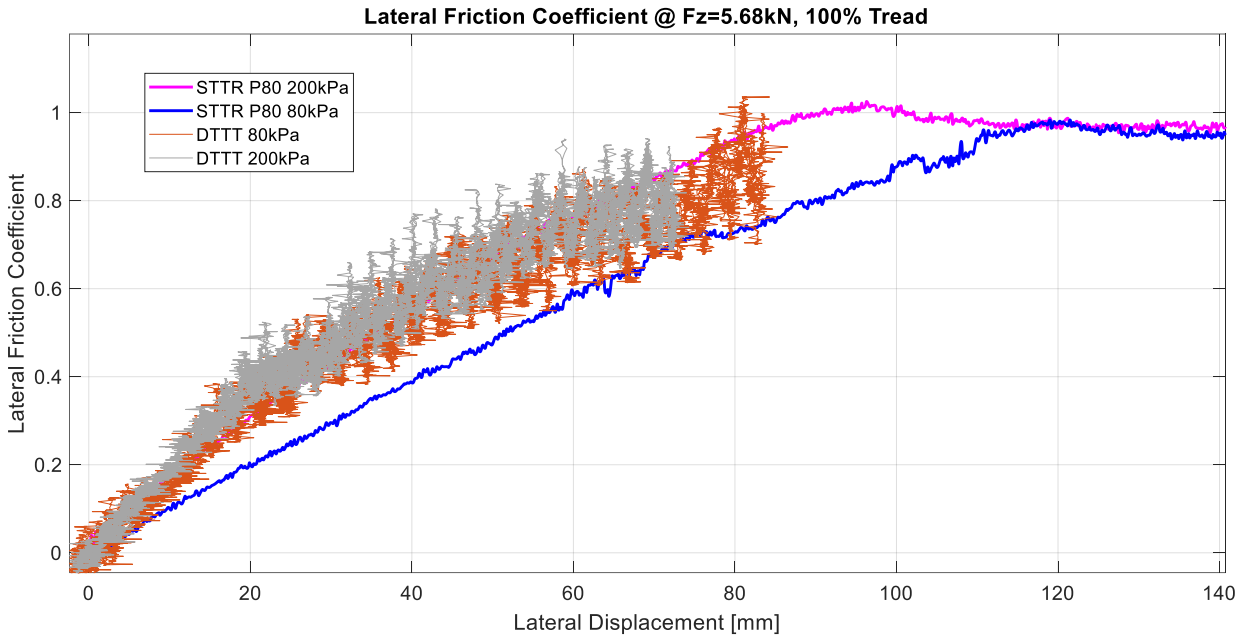

Figure 36: Dynamic lateral friction coefficient tests compared to static testes on P80 at 80kPa and 200kPa inflation pressure for 100% tread, respectively.

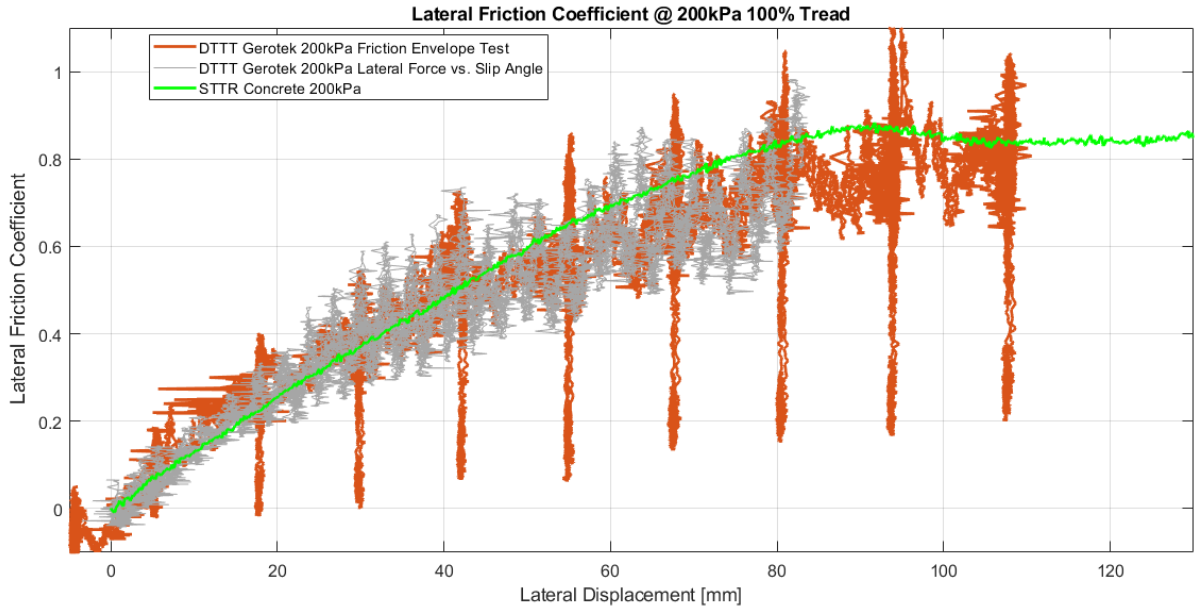

Figure 37: Dynamic lateral friction coefficient tests compared to static testes on concrete at 200kPa inflation pressure for 100% tread.

7. Conclusion

This study presented friction coefficient measurements on different dry non-deformable surfaces in a laboratory and outdoor test tracks. In this study different friction coefficients measurements are presented for the same tyre at three tread wear conditions on different surfaces.

This study has shown the effect that a test surface with a low surface roughness and a high surface roughness will have on the measured tyre characteristics. In general, the test results on concrete surfaces on the static tyre test rig and static trailer tests at Gerotek correlate well when considering the different boundary conditions. It is well known that the friction coefficient on all test surfaces differ in every environment, thus it is suggested that the surface roughness of the test surface, on in which the tyre will be used the most, is measured before tyre characterisation tests are conducted in a laboratory. This surface roughness can then be used to determine which grit

sandpaper or corundum tracks will be best suited to represent the outdoor environment during laboratory tests.

It was found that for the concrete outdoor test surfaces in question the recommended laboratory test surface needs to have a surface roughness value, $10<R_a< 15\mu m$. This roughness is equivalent to a P180 to P220 grit sandpaper, however, using only the sandpaper grade is not a good measure to use. The grading system of sandpaper is based on the number of abrasive particles per square inch on the sandpaper. A more accurate method is to compare the Displacement Spectral Densities of the field test surface with that of the sandpaper intended to use. The spatial frequency of interest that needs to be compared is between 10^4 and 10^6 cycles/m, with corresponding surface index, H2, and roughness coefficient at a spatial frequency of 75 000 cycles/m. The majority of the road surface contains exposed aggregate, which is in direct contact with the rubber in the contact patch, thus the dominating factor in friction generation.

This study has also indicated that stick-slip phenomena is not just possible on smooth surfaces where $R_a<1\mu m$, as stick-slip was measured on surfaces with R_a as high as 3µm. The stick-slip was independent of the size of the contact area and contact pressure in the contact patch. It is concluded that the stick-slip measured on the agricultural tyre of interest was caused by the lower stiffness of the lugs in the tread at 100% tread wear condition.

The results from the dynamic/rolling tyre outdoor tests at a 100% tread condition is successfully compared to the static characterisation tests, with limited success at low inflation pressures due to the tyre belt stiffening for a rolling tyre. This indicates that it is possible to obtain accurate tyre characteristics from static tests which are representative of a rolling tyre at lower velocities and high inflation pressures. This is an important observation as most agricultural vehicles operate at low speeds. This will allow engineers to obtain valuable tyre parameterisation data at a lower cost

with the use of static tyre testing. This data can also be used to parameterise physics-based tyre models for rolling tyre simulations, only when using carefully executed static tests on representative test surfaces.

References

Acuity, 2015. AR700 laser displacement sensor, Oregon: Schmitt Industries.

Ambruster K. and Kutzbach H.D., 1989. Development of a single wheel tester for measurement on driven angled wheel. In: Proceedings of 5th European conference of the ISTVS, Wageningen, The Netherlands; p. 8–14.

American Institute of Physics, 2015. Phys org. [Online] Available at: https://phys.org/news/2015-05-simple-leonardo-da-vinci-combined.html (accessed 14 May 2018).

Becker, C.M. and Els, P.S., 2014, Profiling of rough terrain. International Journal of Vehicle Design, Vol. 64, pp240-261.

Becker, C.M. and Els, P.S., 2018, Static and Dynamic Parameterization Test Rigs for Large Tyres, Proceedings of the 10th Asia-Pacific Conference of the ISTVS, Kyoto, Japan, July 11-13.

Becker, C.M. and Els, P.S., 2020, Motion Resistance Measurements on Large Lug Tyres, Journal of Terramechanics, Vol.88(1), p.17-27.

Becker, C.M. and Els, P.S., 2022, Agricultural Tyre Stiffness Change as a Function of Tyre Wear, Journal of Terramechanics, Vol.102, p.1-15.

Billington P.W., 1973 The NIAE Mk II single wheel tester. J Agric Eng Res; 18:67–70.

Cosin scientific software, 2017, FTire, Modelization and Parameter Specification. 2017-1-r14630. [pdf]. Software documentation and user guide.

Ergun, M., Iyinam, S., and Iyinam A.F., 2005, Prediction of Road Surface Friction Coefficient Using Only Macro- and Microtexture Measurements. Journal of Transport Engineering, 131(4), p 311-319.

Gerotek Test Facilities, 2021, https://www.armscor.co.za/?page_id=3967 , accessed on 16 April 2021.

Gillespie T.D., 1992, Fundamentals of Vehicle Dynamics, p79-120.

Gorsich, D.J., Chaika, M., Gunter, D., Karlsen, R., Haueisen, B., Sun, T. and Ferris, J., 2003, Terrain Roughness Standards for Mobility and Ultra-Reliability Prediction, SAE 2003-01-0218.

Heinrich G. and Klüppel M., 2008, Rubber Friction, Tread Deformation and Tire Traction, Wear, 265:1052-1060.

ISO 4287: 1997, International Organization for Standardization 4287: Geometrical Product Specifications (GPS) , Surface texture: Profiling method – Terms, definitions and surface texture parameters.

ISO 8606: 1995, International Organization for Standardization 8606: Mechanical vibration - Road surface profiles - Reporting of measured data.

ISO 13473: 1997. International Organization for Standardization 13473: Characterization of Pavement Texture by Use of Surface Profiles.

Le Gal, A., Guy, L., Orange, G., Bomal, Y., Klüppel M., 2008. Modelling of Sliding Friction of Carbon Black and dSilica Filled Elastomers on Road Tracks. Wear, Volume 264, Issue 7-8, pp 606-615.

Mitutoyo, 2021, SJ210 Portable Surface Roughness Tester, https://www.mitutoyo.com/wp-content/uploads/2015/08/Surftest_SJ210.pdf, Assessed 23 July 2021.

Persson, B.N.J., 2001, Theory of rubber friction and contact mechanics. Journal of Chemical Physics, vol.115:3840-3860.

Salehi M., Noordermeer J.W.M., Reuvekamp L.A.E.M., Dierkes W.K., Blume A., 2019, Measuring Rubber Friction Using a Laboratory Abrasion Tester (LAT100) to Predict Car Tire Dry ABS Braking. Tribology International, 131, p 191-199.

Scholtz, O. and Els, P.S., 2020, Tyre Rubber Friction on a Rough Road, Journal of Terramechanics, 93:41-50.

Shigley, J.E., 1986, Mechanical Engineering Design, First Metric Edition, Appendix Tables A-9, #5 Simple supports-center load.

Shmuleviuch I., Ronai D., Wolf D., 1996. A new field single wheel tester. Journal of Terramechanics ;33(3):133–41.

Tekscan Pressure Mapping, Force Measurement and Tactile Sensors, 2021, South Boston, MA, USA: https://www.tekscan.com/products-solutions/systems/tirescan-versatek-system, accessed on 9 April 2021.

Witzel, P., 2018. The Hohenheim tyre model: a validated approach for the simulation of high volume tyres – Part I: Model structure and parameterisation. J. Terrramech. 75, 3–14.

Zaayman, O.C.D., 1988, Terrain profile roughness measurement and characterization, Unpublished M.Eng Thesis, University of Pretoria, Pretoria, South Africa.

Zuleeg, J., "How to Measure, Prevent, and Eliminate Stick-Slip and Noise Generation with Lubricants," SAE Technical Paper 2015-01-2259, 2015, doi:10.4271/2015-01-2259.